nature materials

Article

https://doi.org/10.1038/s41563-024-02114-5

Blood–brain-barrier-crossing lipid nanoparticles for mRNA delivery to the central nervous system

Received: 15 June 2023

Accepted: 20 December 2024

Published online: 17 February 2025

Check for updates

Chang Wang[1,2,9], Yonger Xue[1,2,9], Tamara Markovic[3,9], Haoyuan Li[1], Siyu Wang[1], Yichen Zhong[1,2], Shi Du[1,2], Yuebao Zhang[2], Xucheng Hou[1,2], Yang Yu[2], Zhengwei Liu[1], Meng Tian[1], Diana D. Kang[1,2], Leiming Wang[1], Kaiyuan Guo[1], Dinglingge Cao[1], Jingyue Yan[1,2], Binbin Deng[4], David W. McComb[4,5], Ramon E. Parsons[6], Angelica M. Minier-Toribio[3], Leanne M. Holt[3], Jiayi Pan[7], Alice Hashemi[8], Brian H. Kopell[8], Alexander W. Charney[8], Eric J. Nestler[3] ✉, Paul C. Peng[7] ✉ & Yizhou Dong[1,2] ✉

The systemic delivery of mRNA molecules to the central nervous system is challenging as they need to cross the blood–brain barrier (BBB) to reach into the brain. Here we design and synthesize 72 BBB-crossing lipids fabricated by conjugating BBB-crossing modules and amino lipids, and use them to assemble BBB-crossing lipid nanoparticles for mRNA delivery. Screening and structure optimization studies resulted in a lead formulation that has substantially higher mRNA delivery efficiency into the brain than those exhibited by FDA-approved lipid nanoparticles. Studies in distinct mouse models show that these BBB-crossing lipid nanoparticles can transfect neurons and astrocytes of the whole brain after intravenous injections, being well tolerated across several dosage regimens. Moreover, these nanoparticles can deliver mRNA to human brain ex vivo samples. Overall, these BBB-crossing lipid nanoparticles deliver mRNA to neurons and astrocytes in broad brain regions, thereby being a promising platform to treat a range of central nervous system diseases.

Messenger RNA (mRNA) has been explored for a number of applications, such as vaccines, cancer immunotherapies and protein replacement therapies[1–7]. To realize these applications, lipid nanoparticles (LNPs) are emerging as a safe and effective delivery platform from bench to clinic. In particular, LNP-mRNA vaccines were rapidly developed and used against the COVID-19 pandemic in 2020 (refs. 8–11). In general, many LNPs after systemic administration deliver mRNA to the liver. Recently, several approaches have been developed to deliver mRNA to other tissues, such as the pancreas, eyes, lungs, uterus and testes[12–17]. However, the delivery of mRNA to the brain remains a formidable challenge due to the blood–brain barrier (BBB)[18,19].

In essence, the BBB consists of pericytes, astrocytic processes and a basement membrane that surrounds a monolayer of endothelial cells that constitute the brain's vascular supply[20–24]. This physiological barrier selectively blocks the passage of many small molecules, proteins and mRNA into the brain. Previous studies have reported that several approaches can mediate the crossing of the BBB, including passive diffusion and adsorptive-mediated, carrier-mediated and receptor-mediated transcytosis[25]. On the basis of the findings of these natural transportation pathways, researchers have explored many strategies to deliver various types of functional cargos to the brain. For example, silica nanoparticles conjugated with glucose and glycoprotein

A full list of affiliations appears at the end of the paper. ✉e-mail: eric.nestler@mssm.edu; paul.peng@biogen.com; yizhou.dong@mssm.edu

peptides were reported to deliver genome-editing components to the brain by retro-orbital injection[26]. An mRNA-loaded exosome with brain tumour-targeting peptides was used to treat orthotopic glioblastoma (GBM)[27]. Fucoidan-based nanoparticles were developed to undergo caveolin-1-dependent transcytosis and cross the BBB[28]. Despite these significant advances, there is an urgent demand to effectively and safely deliver mRNA to brain cells, especially neurons.

To achieve mRNA delivery in the brain, new strategies need to be conceived. Previously, researchers reported that certain small-molecule ligands can cross the BBB through diverse pathways. Specifically, L-DOPA can be recognized by the large neutral amino acids transporter 1 on endothelial cells and be transported across the BBB for the treatment of Parkinson's disease[29–31]. D-Serine serves as a neuromodulator and crosses the BBB by amino acid transporter solute carrier family 6 member 14 (refs. 31–35). Temozolomide is an alkylating lipophilic agent that crosses the BBB to treat GBM[36,37]. Tryptamine derivatives are neurotransmitter precursors that cross the BBB by active transport via Mg^{2+} and ATP-dependent uptake[38–40]. Cinnamic derivatives can cross the BBB and insert into the beta sheet of amyloid β proteins[41]. MK-0752 reduces the generation of amyloid-β after crossing the BBB in vivo[42,43]. On the basis of these important findings, we designed and synthesized six classes of BBB-crossing lipids (BLs) by conjugating these molecules with various amino lipids. We hypothesize that these BLs can facilitate formulations of BBB-crossing lipid nanoparticle (BLNP) with mRNA that cross the BBB and efficiently deliver mRNA to the central nervous system (Fig. 1a).

Design and development of BLNPs for systemic mRNA delivery to the brain

Inspired by the structures and functions of small-molecular ligands that can cross the BBB, we designed six classes of BLs (Fig. 1b) including L-DOPA-derived lipids (LD), D-serine-derived lipids (DS), temozolomide-derived lipids (TM), tryptamine-derived lipids (TD), cinnamic-acid-derived lipids (CD) and MK-0752-derived lipids (MK). These BLs consist of various amino groups and lipid chains. We incorporated diverse functional groups in the chains such as ester, carbonate and acetal. On the basis of the unique structures of these BLs, we conceived the synthesis routes for individual lipids. Figure 1c shows the representative synthesis of DS11 and MK6. For example, D-serine was first protected by Fmoc to give Fmoc-D-serine. Then, Fmoc-D-serine was coupled to Boc-protected diethylenetriamine, followed by the deprotection of Boc to obtain compound **1**. Finally, compound **1** underwent reductive amination with lipid aldehydes and subsequent deprotection to afford DS11. Through a separate synthesis pathway, Boc-protected hexamethylenediamine was condensed with MK-0752, followed by the subsequent deprotection of Boc to give compound **2**. Last, a reductive amination reaction between compound **2** and an aldehyde produced MK6. All the compounds were purified by flash chromatography and validated by ^{1}H nuclear magnetic resonance and mass spectrometry.

Next, we formulated each BL with firefly luciferase (FLuc) mRNA to generate BLNPs, and studied their physicochemical properties. The particle sizes of BLNPs ranged from 97.3 ± 2.0 nm to 177.6 ± 2.0 nm with a polydispersity index of <0.3 (Supplementary Fig. 1a,b). They are positively charged and the obtained mRNA encapsulation efficiency ranges from 64.9 ± 4.1% to 88.1 ± 5.0% (Supplementary Fig. 1b). Then, we evaluated their mRNA delivery efficiency in Neuro-2a (N2a), a mouse neuroblastoma cell line, and bEnd.3, a mouse brain endothelial cell line. A series of BLNPs showed over fivefold higher luminescence intensity than DLin-MC3-DMA (MC3) LNPs in N2a cells (Fig. 2a–f). In particular, CD6, TD5, TD8 and MK6 BLNPs showed over tenfold higher luminescence intensity than MC3 LNPs. Moreover, these lead BLNPs also exhibited high mRNA delivery efficiency in bEnd.3 cells (Supplementary Fig. 2a–f). Meanwhile, these BLNPs displayed minimal toxicity in both N2a and bEnd.3 at the tested dose (80% or higher cell viability in all the treated groups; Supplementary Fig. 3a,b). Additionally, we measured the apparent pKa of BLNPs, an important parameter of LNP. Their apparent pKa ranged from 5.28 to 9.79 (Supplementary Fig. 4a–f). We further analysed the structure–activity relationships of these BLNPs based on the data from the N2a cells. For example, LDs with two hydrocarbon tails possessed better delivery efficacy than LDs with three and four tails. Specifically, LD10 BLNPs bearing two tails with a carbonate ester were the most effective in mRNA delivery, which was 4.7-fold greater than MC3 LNPs. Similarly, among the DSs, DS11 BLNPs (equipped with carbonate ester tails) showed 6.9-fold higher luminescence intensity than MC3 LNPs. In the series of CD lipids, CD6 with three acetal tails showed 14.4-fold higher luminescence intensity compared with MC3 LNPs. By contrast, the luminescence intensity in TMs was relatively low. In the case of TDs, the length of the hydrocarbons greatly affected the delivery efficiency of mRNA. TD5, installed with myristic hydrocarbon tails, exhibited better delivery efficiency than those with palmitic and lauric tails. TD8 with three acetal tails showed 13.4-fold higher luminescence intensity than MC3 LNPs. For the MK lipid series, 14.6-fold higher luminescence intensity was found for MK6 with acetal tails compared with MC3. These results suggest that both BBB-crossing modules and diverse structures of amino lipids can greatly affect the in vitro mRNA delivery efficiency.

On the basis of these in vitro results, 12 lead BLNPs were selected for further in vivo evaluation. These 12 BLNPs showed the highest luciferase activity among all the BLNPs tested in both N2a cells and bEnd.3 cells. We formulated these BLNPs with FLuc mRNA and injected them intravenously into mice at an mRNA dose of 0.5 mg kg^{-1} via the tail vein. Among all the BLNPs tested, MK6 BLNPs induced the highest luminescence intensity in brain tissue 6 h after administration, which was much higher than MC3 LNPs (Fig. 2g,h). Both MK6 BLNPs and MC3 LNPs showed similar signal intensity in other major organs (Fig. 2i and Supplementary Fig. 5a). We did not observe a correlation between particle size and biodistribution. Meanwhile, we characterized the particle properties of MK6 BLNPs using several well-established methods. MK6 BLNPs were around 139.8 ± 3.5 nm in diameter with a polydispersity index of <0.15 (Supplementary Fig. 5b). Approximately 83.1 ± 2.7% of mRNA was encapsulated in MK6 BLNPs, and they were slightly positively charged (Supplementary Fig. 5c).

Optimization of BLNPs for systemic mRNA delivery to the brain

To further improve the brain delivery efficiency of BLNPs through systemic administration, we conducted several rounds of experiments to optimize MK6 BLNP formulations (Supplementary Fig. 6a). In our prior studies, we found that the increase in ionizable lipid molar ratio in the LNP formulation can augment mRNA delivery[44]. Therefore, we increased the molar ratios of MK6 in the formulation, ranging from 20 to 60, and maintained the other parameters constant. As the molar ratios of MK6 increased, we observed MK6B BLNPs (a molar ratio of MK6/1,2-dioleoyl-*sn*-glycero-3-phosphoethanolamine (DOPE)/cholesterol/1,2-dimyristoyl-rac-glycero-3-methoxypolyethylene glycol-2000 ($DMG\text{-}PEG_{2k}$) = 60:30:40:0.75) with a slight improvement in luminescence intensity in the brain (intravenous, tail-vein injection; mRNA dose, 0.5 mg kg^{-1}; Fig. 3a). This specific molar ratio was selected for subsequent optimization rounds. Next, by adjusting the weight ratios between MK6 and mRNA, we found that MK6E BLNPs with a weight ratio of MK6/mRNA = 12.5/1 showed a twofold increase in brain luminescence intensity compared with the original MK6 BLNPs (Fig. 3a,b). Thus, this formulation composition—BL/DOPE/cholesterol/$DMG\text{-}PEG_{2k}$ = 60:30:40:0.75 and BL/mRNA = 12.5/1—was chosen for the following studies.

In addition to tuning the formulation ratios, we modified the chemical structure of MK6 by adjusting the length of the alkyl chains and the position of acetal groups in the lipid tails, which led to the synthesis of MK13-MK16 BLs (Fig. 3c). These MK BLNPs exhibited similar particle size, encapsulation efficiency and zeta potential (Supplementary

https://doi.org/10.1038/s41563-024-02114-5

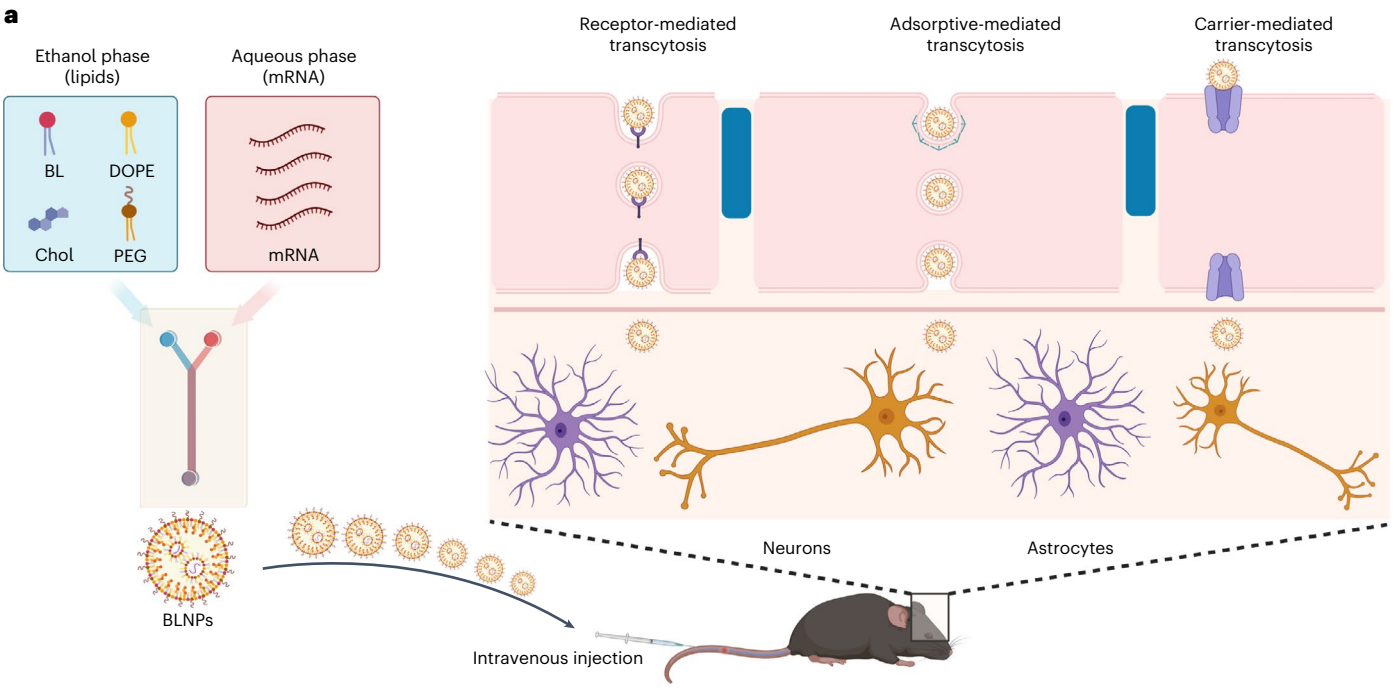

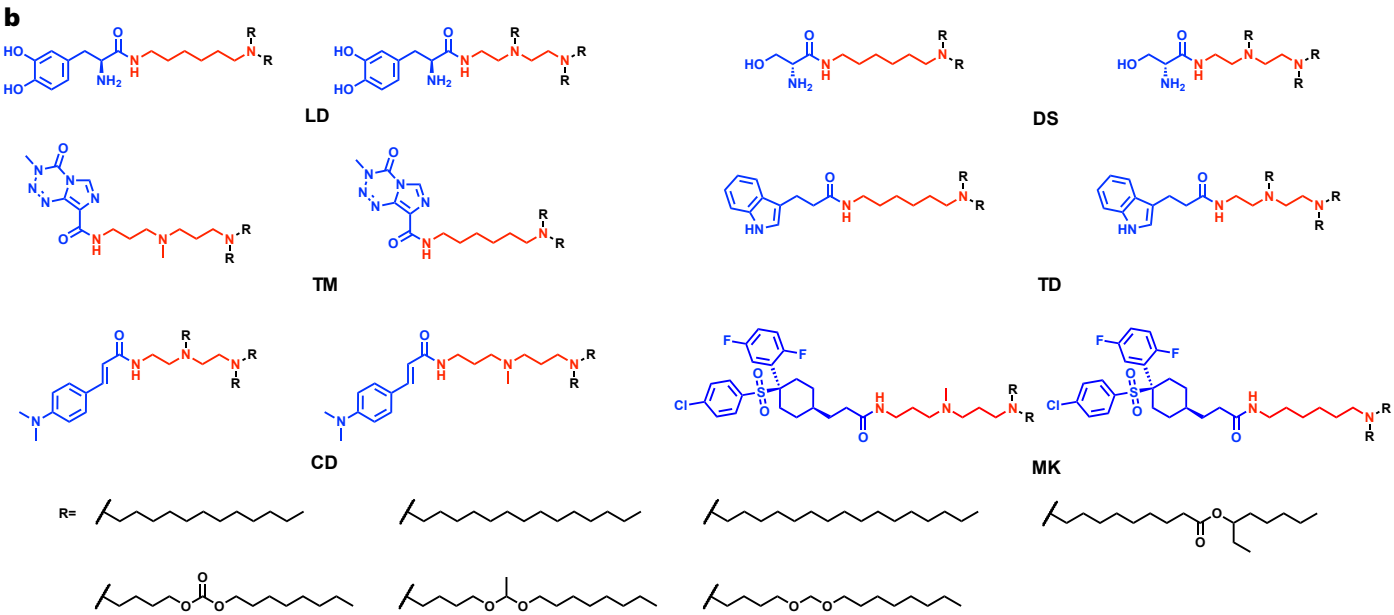

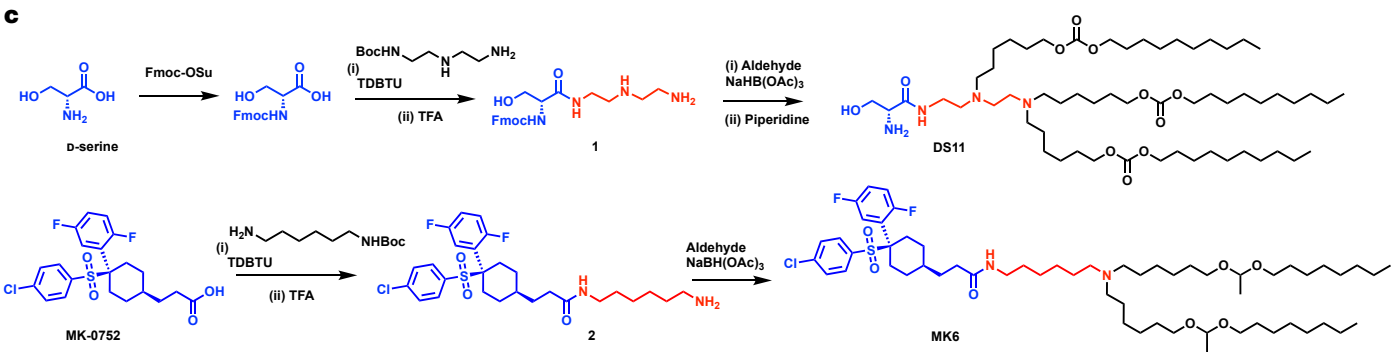

Fig. 1 | Design of BLNPs. a, Illustration of the formulation of BLNPs and potential BBB-crossing mechanisms. **b**, Chemical structures of BLs. **c**, Synthesis routes of representative BLs (DS11 and MK6).

https://doi.org/10.1038/s41563-024-02114-5

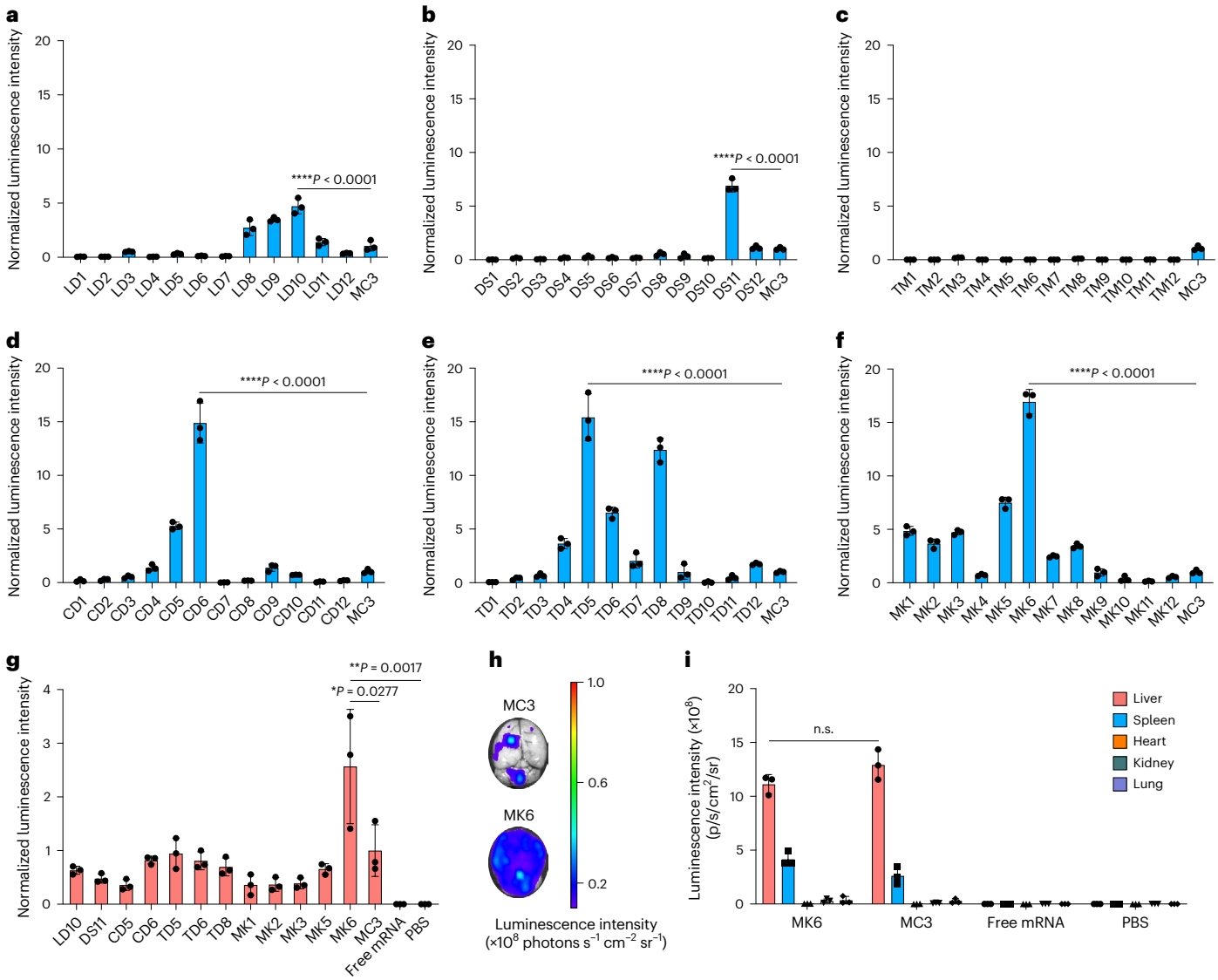

Fig. 2 | Characterizations of BLNPs for mRNA delivery. a–**f**, Luminescence intensity of BLNP-FLuc mRNA in N2a cells. The intensity was normalized to the MC3 LNP group. **g**, Luminescence intensity of brains from the lead BLNP-FLuc-mRNA-treated mice (intravenous). The intensity was normalized to the MC3 LNP group. **h**, Representative images of brains from the mice intravenously treated with MC3 LNPs and MK6 BLNPs. **i**, Luminescence quantification of the organs from mice treated with PBS, free mRNA, MC3 LNP or MK6 BLNP. Data in **a**–**i** are from $n = 3$ biologically independent samples. Data are presented as mean ± s.d. Statistical significance was determined by one-way ANOVA followed by Dunnett's multiple comparisons test. n.s., not significant, $P > 0.05$, $^{*}P < 0.05$, $^{**}P < 0.01$, $^{****}P < 0.0001$.

Fig. 6b,c). They also presented similar apparent pKa values, with a narrow range from 6.70 to 6.99 (Supplementary Fig. 6d). Among this series of MK BLNPs, MK16 BLNPs showed the highest in vivo luminescence intensity in the mouse brain after intravenous injection, which was 1.7-fold higher than MK6E BLNPs and 8.3-fold greater than MC3 LNPs (Fig. 3d,e). These results suggest that the alkyl chain length surrounding the acetal group greatly affected the mRNA delivery efficiency of MK BLNPs to the brain. Moreover, MK6, MK6E and MK16 displayed comparable distribution trends in other major organs (Supplementary Fig. 7a,b). Additionally, MK16 BLNPs showed 7.4-fold and 6.5-fold higher luminescence intensity than ALC-0315 and SM-102 LNPs in brains after intravenous administration, respectively (Supplementary Fig. 8a,b). The MK16 BLNPs exhibited a particle size of 137.0 ± 4.1 nm and an mRNA encapsulation efficiency of approximately 84.8 ± 1.5% (Supplementary Fig. 9a,b). The particles were positively charged and displayed spherical morphology in cryogenic transmission electron microscopy images (Supplementary Fig. 9c). Additionally, MK16 BLNPs showed potent mRNA delivery efficiency in both bEnd.3 cells and N2a cells with negligible cytotoxicity at the tested dose (Supplementary Fig. 9d,e). On the basis of the above results, we selected MK16 BLNPs as the leading material for further studies.

To assess the kinetics of MK16 BLNPs delivery to brain, we measured the fluorescence intensity of MK16 BLNPs loaded with an Alexa Fluor 647-labelled RNA at different time points following a single intravenous injection. Substantial levels of fluorescent signals were observed in the brain at the time points of 1 h and 6 h, with no detectable signals at and after the 18 h time point (Supplementary Fig. 10a). Moreover, we calculated the percentages of fluorescent signals ending up in major organs after an intravenous injection of MK16-Alexa 647 RNA BLNPs. Using this method, we observed nearly 56.6 ± 2.5% of the MK16 BLNPs in the liver, 6.5 ± 1.1% in the spleen, 7.4 ± 0.8% in the kidneys, 10.5 ± 1.0% in the lungs and 3.7 ± 1.4% in the heart (Supplementary Fig. 10b). In particular, there was 15.3 ± 0.4% of the MK16 BLNPs in the brain.

https://doi.org/10.1038/s41563-024-02114-5

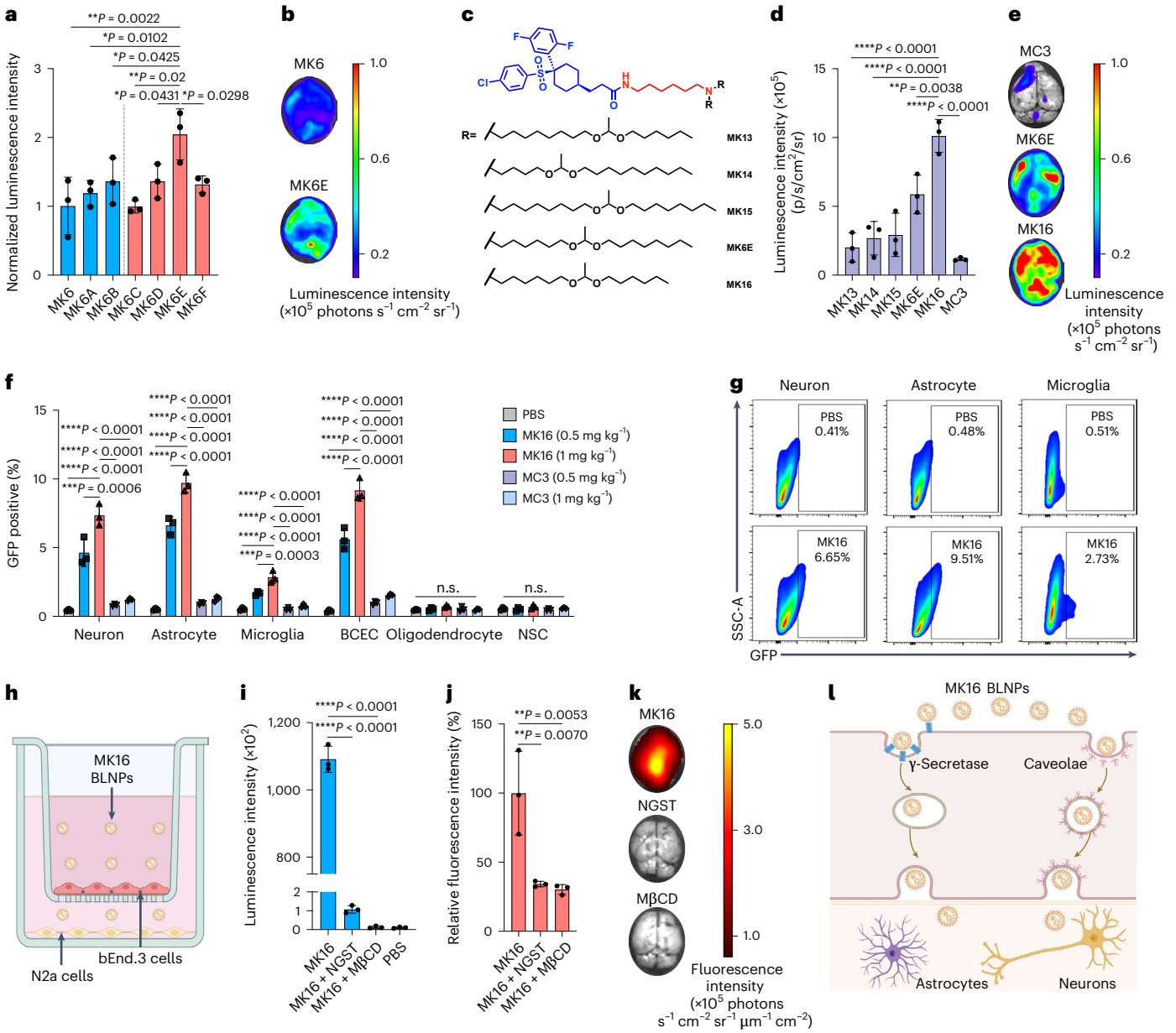

Fig. 3 | Optimization and characterization of MK6 BLNP series for systemic mRNA delivery to mouse brain. a,**b**, Normalized luminescence intensity (**a**) and representative IVIS images (**b**) of brains of mice intravenously injected with MK6 BLNPs and MK6E BLNPs encapsulating FLuc-mRNA. The intensity was normalized to the MK6 BLNP group. **c**, Structure optimization of MK6 BLs. **d**,**e**, Normalized luminescence intensity (**d**) and representative images (**e**) of brains after intravenous injections with MC3 LNPs, MK6E BLNPs or MK16 BLNPs. The intensity was normalized to the MC3 LNP group. **f**, Immunofluorescence flow cytometry analysis of GFP expressions in different brain cell types from brains of the mice intravenously injected with MK16 BLNP-GFP mRNA or MC3 LNP-GFP mRNA. **g**, Representative histograms of GFP expression in different brain cell types after various doses of MK16-mediated GFP mRNA delivery (1 mg kg^{-1}) from **f**. **h**, Illustration of a bEnd.3-N2a transwell cell assay for BBB penetration assessment. The lower compartment was seeded with N2a cells. **i**, Luminescence intensity of N2a cells in the lower compartment after MK16 BLNP-FLuc mRNA treatment to the bEnd.3 cells in the upper compartment. The bEnd.3 cells were pretreated with either MβCD or NGST. **j**,**k**, Fluorescence intensity (**j**) and representative IVIS images (**k**) of the brains of the mice after intravenous injections with MK16 BLNPs encapsulating Alexa Fluor 647-labelled RNAs. The mice were pretreated with either MβCD or NGST. **l**, Illustration of the proposed BBB-crossing mechanisms of MK16 BLNPs. All data are from $n = 3$ biologically independent samples and are presented as mean ± s.d. Statistical significance and P values were determined by one-way ANOVA followed by Dunnett's multiple comparisons test. n.s., not significant, $P > 0.05$, $^{**}P < 0.01$, $^{***}P < 0.001$, $^{****}P < 0.0001$.

To investigate MK16 BLNPs for mRNA delivery in different types of brain cell in vivo, we formulated MK16 BLNPs with mRNA encoding green fluorescent protein (GFP) and conducted a single intravenous injection of the formulation in mice. Then, we quantified the cellular distribution through the flow cytometry analysis of brain tissues 12 h after administration (Supplementary Fig. 11a). MK16 BLNPs preferentially delivered GFP mRNA to neurons (4.64 ± 1.00% GFP$^+$), astrocytes (6.63 ± 0.62% GFP$^+$) and brain capillary endothelial cells (BCECs; 5.62 ± 0.78% GFP$^+$) at an mRNA dose of 0.5 mg kg^{-1}, the efficiency of which is particularly superior to those achieved by MC3 LNPs in the corresponding cell types (Fig. 3f,g and Supplementary Fig. 11b). Additionally, a small proportion of microglia (1.68 ± 0.15% GFP$^+$) also exhibited GFP expression. By contrast, oligodendrocytes and neural stem cells showed negligible GFP expression. Furthermore, increasing

the dose of GFP mRNA to 1 mg kg^{-1} led to enhanced GFP expression in neurons (7.36 ± 0.78%), astrocytes (9.71 ± 0.70%), BCECs (9.18 ± 0.80%) and microglia (2.85 ± 0.44%), suggesting the mRNA delivery efficiency of MK16 BLNPs to brain cells is dose dependent (Fig. 3f,g and Supplementary Fig. 11b).

Mechanisms of MK16 BLNP across the BBB

To explore the possible mechanisms of BBB transportation by MK16 BLNPs, we constructed a transwell assay consisting of bEnd.3 cells to mimic the BBB using the method reported before (Supplementary Fig. 12a)[45]. In this model, MK16 BLNPs encapsulated with Alexa Fluor 647-labelled RNA exhibited dramatically higher fluorescence intensity in the lower compartment than the groups of phosphate-buffered saline (PBS) and MC3 LNPs, respectively (Supplementary Fig. 12b). When methyl-beta-cyclodextrin (MβCD; a caveolae-mediated endocytic inhibitor) was used to pretreat cells, a 43.3 ± 1.7% decrease in transcytosis efficiency was observed (Supplementary Fig. 12c). However, treatment with chlorpromazine (a clathrin-mediated endocytic inhibitor) and 5-(*N*-ethyl-*N*-isopropyl)-amiloride (a micropinocytosis-mediated endocytic inhibitor) did not significantly reduce the transcytosis efficiency of MK16 BLNPs. Furthermore, pretreatment with MK-0752, the small molecule incorporated as the BBB-crossing module in MK lipids, resulted in a 63.8 ± 3.1% decrease in the transcytosis efficiency of MK16 BLNPs, indicating that MK-0752 competitively inhibited the transcytosis of MK16 BLNPs (Supplementary Fig. 12c). This finding suggested that MK16 BLNPs may partially utilize the transportation mechanism used by MK-0752 molecules. Since MK-0752 is a γ-secretase inhibitor, we speculated that γ-secretase may facilitate the transcytosis of MK16 BLNPs through bEnd.3 cells. Therefore, we added nirogacestat (NGST)—an FDA-approved γ-secretase inhibitor—to the transwell assay as well as the seeded N2a cells in the lower compartment to examine whether MK16 BLNPs could cross the endothelial cell layer and then deliver FLuc mRNA to the N2a cells after transcytosis. Co-incubation with MβCD or NGST sharply diminished the luminescence intensity in both bEnd.3 cells in the upper compartment and N2a cells in the lower compartment, compared with the groups treated only by MK16 BLNPs (Fig. 3h,i and Supplementary Fig. 12d). These results indicate that MK16 BLNPs can cross endothelial cells by both caveolae- and γ-secretase-mediated transcytosis. To further validate the mechanism in vivo, we pretreated mice with either MβCD or NGST before intravenous administrations of MK16 BLNPs loaded with an Alexa Fluor 647-labelled RNA. As shown in Fig. 3j,k, both MβCD and NGST resulted in a significant decrease in fluorescence intensity in the brains of pretreated mice compared with those receiving only MK16 BLNPs, suggesting a substantial reduction in the passage of MK16 BLNPs across the BBB. These findings demonstrate that caveolae and γ-secretase might be critical mediators in facilitating the BBB crossing of MK16 BLNPs.

Delivery applicability and safety studies of MK16 BLNPs

We next investigated MK16 BLNPs for functional mRNA delivery in an Ai14 mouse model (Fig. 4a). The Ai14 mouse is genetically engineered with a LoxP-flanked stop cassette that prevents tdTomato expression in vivo at the baseline, but activates the tdTomato expression with Cre recombinase[46]. In this experiment, we evaluated Cre recombinase mRNA-mediated editing by intravenously administering MK16 BLNPs to Ai14 mice. In PBS-treated mice, tdTomato expression was undetectable 5 days after administration, but on MK16 BLNP delivery of Cre mRNA, a tdTomato signal was observed throughout most regions of the brain, with the strongest signal detected in brain margins (Fig. 4b and Supplementary Fig. 13a,b). These areas are adjacent to the meninges, which consist of abundant blood vessels. By contrast, MC3 LNPs resulted in a negligible tdTomato signal, indicating a markedly lower efficiency in delivering Cre mRNA throughout the brain. Importantly, an obvious tdTomato signal was observed in the hippocampus, thalamus and cerebral cortex of the brains from Ai14 mice treated with MK16 BLNP-Cre mRNA (Fig. 4c–e). The expression levels of tdTomato-positive cells were comparable in these three brain regions. Specifically, in the hippocampus, tdTomato-positive neurons in the MK16 BLNP group accounted for 5.98 ± 1.52% of the total, whereas in the thalamus and cortex, the proportions were 5.86 ± 0.42% and 6.68 ± 1.13%, respectively (Fig. 4f–h). Astrocytes with the tdTomato signal represented 8.36 ± 1.85% in the hippocampus, 8.49 ± 1.53% in the thalamus and 8.74 ± 2.07% in the cortex (Fig. 4f–h). In the MC3 LNP group, the neurons and astrocytes displaying the tdTomato signal within the hippocampus, thalamus and cerebral cortex regions were observed at approximately 1% (Fig. 4f–h). To study whether multiple injections of MK16 BLNP-Cre mRNA could enhance gene editing in Ai14 mice, we compared the tdTomato expression levels across various brain cell types from the mice receiving single or triple injections of MK16 BLNPs. The results showed that triple injections of MK16 BLNPs resulted in approximately twofold higher tdTomato expression in neurons, astrocytes, BCECs and microglia than those in the single-injection group (Fig. 4i). Specifically, the tdTomato expression level of these brain cells after three injections was quantified as 16.7 ± 2.2% in neurons, 19.2 ± 3.0% in astrocytes, 17.9 ± 1.6% in BCECs and 4.5 ± 0.9% in microglia. Moreover, the tdTomato signals in these brain cells induced by MK16 BLNPs were much higher than MC3 LNPs in both single- and triple-injection groups. Together, these results highlight the potential of MK16 BLNPs as promising mRNA carriers to cross the BBB, deliver multiple types of mRNA to essential brain cells (especially neurons and astrocytes) and induce robust expression of functional proteins across broad regions of the brain.

Next, we conducted a series of experiments to understand the safety profile of MK16 BLNPs. Since MK-0752—a starting material for the chemical synthesis of MK16—is a potent NOTCH inhibitor, we investigated whether MK16 BLNPs might regulate NOTCH pathways in various organs[47,48]. In this work, we applied an RNA-sequencing assay to profile the expression level of NOTCH-related mRNA transcripts in the brain, liver and spleen. As shown in Supplementary Fig. 14a, mice treated with MK16 BLNPs displayed expression levels of most NOTCH genes that were similar to those in the PBS-treated group. By contrast, mice treated with MK-0752 exhibited substantial alterations in certain key NOTCH-related transcripts. To further study the potential toxicity and cytokine profiles of MK16 BLNPs, we collected plasma samples from the treated mice at intervals of 6, 24 and 48 h post-administration for comprehensive blood biochemical analysis. The proinflammatory cytokine and chemokine profiles elicited by MK16 BLNPs were comparable with or milder than those induced by MC3 LNPs at the same mRNA dose (Supplementary Fig. 14b). The levels of most biomarkers in both groups reverted to the baseline, as established by the PBS control, at 24 and 48 h after injection (Supplementary Fig. 14b,c). To assess the effects of MK16 BLNPs on liver and kidney function, plasma samples were also analysed for key biomarkers indicative of metabolic and excretory processes. The levels of aspartate aminotransferase, alanine aminotransferase and blood urea nitrogen remained within the normal range, suggesting that the hepatic and renal functions were not adversely affected by the administration of MK16 BLNPs (Supplementary Fig. 14d). Furthermore, thorough histopathological evaluations of harvested tissues including the brain, heart, liver, lungs, spleen and kidneys at various time intervals revealed no notable pathological alterations (Supplementary Figs. 14e, 15 and 16). Finally, blood biochemical analysis and histopathological evaluations of major organs of the Ai14 mice revealed that multiple injections of MK16 BLNPs did not elicit obvious systemic toxicity (Supplementary Fig. 17a–d). These results highlight the biocompatibility and safety of MK16 BLNPs.

Demonstration of MK16 BLNPs in a cocaine exposure model

After the validation of delivery efficiency and tolerability of MK16 BLNPs, we probed their ability to deliver a functional mRNA in a

https://doi.org/10.1038/s41563-024-02114-5

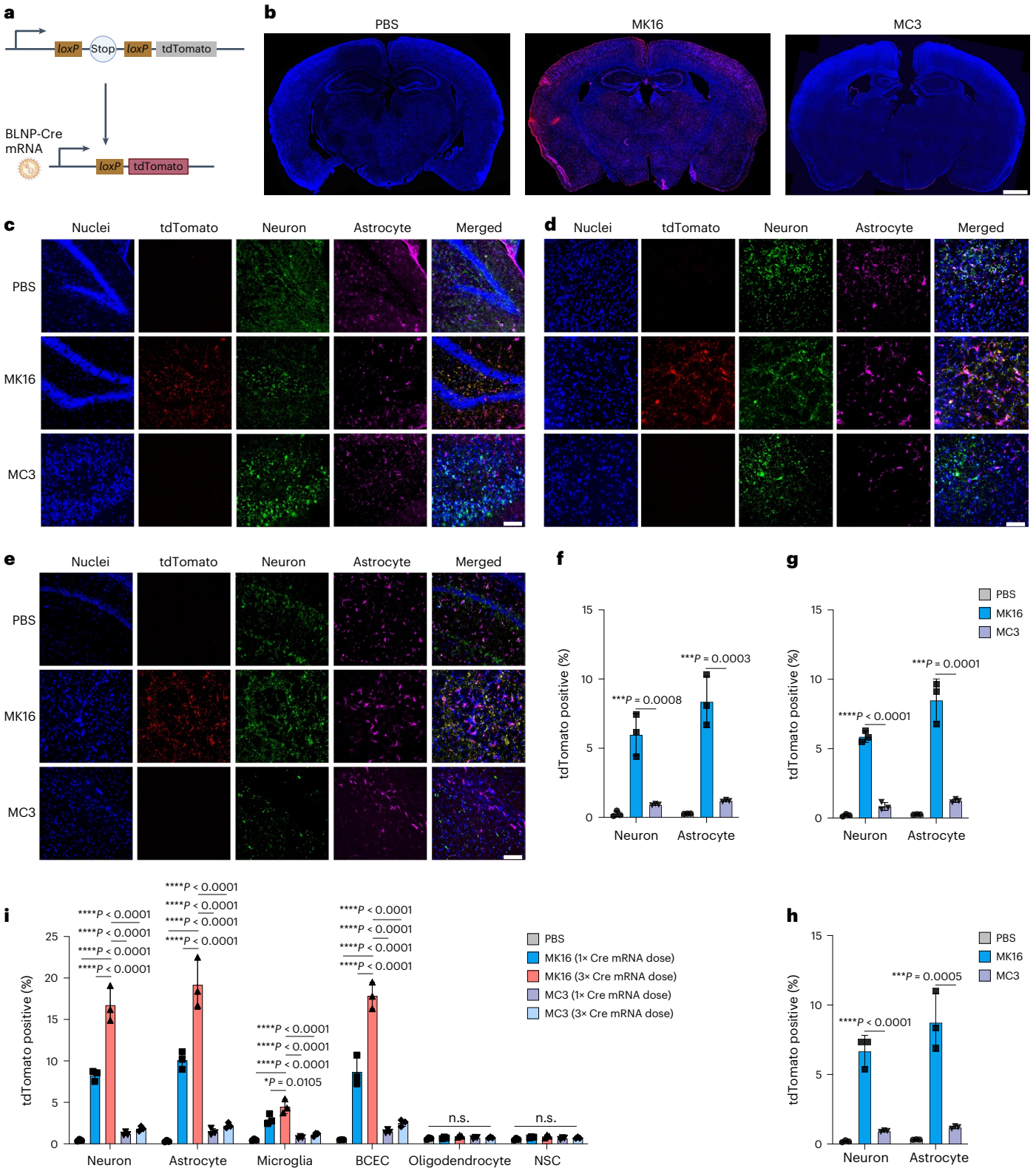

Fig. 4 | MK16 BLNPs for Cre mRNA delivery in the Ai14 mouse model. a, Diagram depicting that delivery of Cre recombinase mRNA turns on tdTomato expression in Ai14 mice. **b**, Representative brain images of Ai14 mice intravenously injected with PBS, MK16 BLNP-Cre mRNA or MC3 LNP-Cre mRNA. Scale bar, 1 mm. **c**–**e**, tdTomato expression in neurons (Map2$^+$) and astrocytes (GFAP$^+$) in the hippocampus (**c**), thalamus (**d**) and cortex (**e**). Scale bar, 50 µm. **f**–**h**, Quantification of tdTomato-positive neurons and astrocytes in the hippocampus (**f**), thalamus (**g**) and cortex (**h**). **i**, Immunofluorescence flow cytometry analysis of tdTomato expression in different brain cell types after single or triple intravenous injections of MK16 BLNP-Cre mRNA and MC3 LNP-Cre mRNA. All data are from $n = 3$ biologically independent samples and are presented as mean ± s.d. Statistical significance and P values were determined by one-way ANOVA followed by Dunnett's multiple comparisons test. n.s., not significant, $P > 0.05$, $^{**}P < 0.01$, $^{***}P < 0.001$, $^{****}P < 0.0001$.

https://doi.org/10.1038/s41563-024-02114-5

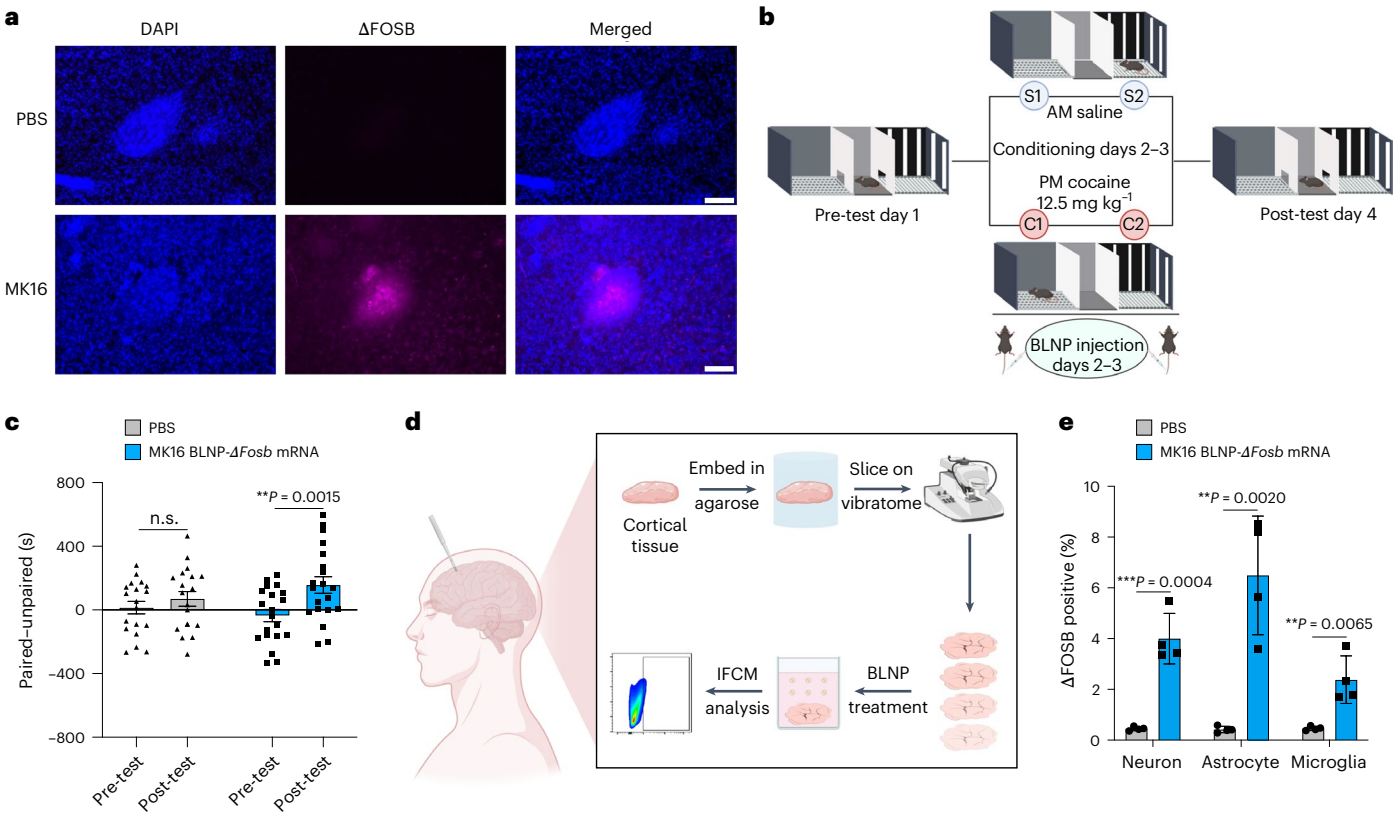

Fig. 5 | MK16 BLNPs for *ΔFosb* mRNA delivery in a CPP model. a, ΔFOSB expression in the NAc region of the mouse brain after the intravenous administration of MK16 BLNP-*ΔFosb* mRNA. Scale bar, 100 µm. $n = 3$ biologically independent samples. **b**, Schematic depicting the CPP procedure. S, saline; C, cocaine. **c**, Preference score calculated as time spent on the drug-paired side − time spent in the saline-paired side of the conditioned mice treated with PBS or MK16 BLNP-*ΔFosb* mRNA. $n = 19$ mice for the PBS group and $n = 20$ mice for the MK16 BLNP group. **d**, Schematic depicting ex vivo mRNA delivery in human brain tissue. IFCM, immunofluorescence flow cytometry. **e**, ΔFOSB expression levels across neurons, astrocytes and microglia from adult human cerebral cortex dissections after ex vivo treatment with PBS or MK16 BLNP-*ΔFosb* mRNA. $n = 4$ tissue slices for each group. Data in **c** and **e** are presented as the mean ± s.d. Statistical significance and P values in **c** were determined by two-way ANOVA with Šidák post hoc test. Statistical significance and P values in **e** were determined by a two-tailed Student's t-test. n.s., not significant, $P > 0.05$, $^{**}P < 0.01$, $^{***}P < 0.001$.

disease model. ΔFOSB is a pivotal transcription factor involved in the regulation of addictive behaviours and the neuropathology of drug dependence[49,50]. Given that the major clinical problem in addiction is that the user becomes tolerant to the effects of the drug over time, prior studies reported that enhancing ΔFOSB could be a viable approach to treat drug addiction by making subthreshold, non-reinforcing doses of cocaine more reinforcing, potentially reducing the risks of overdose[51]. Therefore, we formulated MK16 BLNPs with mRNA encoding ΔFOSB (*ΔFosb* mRNA) and tested this formulation in a cocaine-induced conditioned place preference (CPP) model, which provides an indirect measure of drug reward, to assess the effects of ΔFOSB overexpression in modulating an animal's ability to form drug-context associations. We first studied whether MK16 BLNPs could deliver *ΔFosb* mRNA to the nucleus accumbens (NAc), a key brain reward region in which ΔFOSB is known to exert its most prominent effects[49,50]. Systemic delivery of *ΔFosb* mRNA using MK16 BLNPs resulted in a strong expression of ΔFOSB protein within the NAc 24 h after injection (Fig. 5a). By contrast, negligible ΔFOSB signals were observed in PBS-treated mice. The observed differential expression highlights the capacity of MK16 BLNPs to deliver functional mRNA to deep regions of the forebrain.

Once we observed the reliable production of ΔFOSB driven by MK16 BLNPs in the NAc, we tested its effects in the cocaine-induced CPP model (Fig. 5b). Briefly, animals first underwent a pre-test during which the baseline preferences of wild-type naive mice were established. During the pre-test, animals freely explored a CPP chamber consisting of two distinct compartments (stripe walls with a small mesh floor and dark walls with large mesh floors). Animals were then counterbalanced for drug or saline conditioning to adjust for small-chamber biases across groups. During two consecutive conditioning days, mice received one daily intraperitoneal injection of saline in the morning, and were confined to one chamber for 30 min. In the afternoon, mice received an intraperitoneal injection of a subthreshold dose of cocaine and were confined to the opposite side of the chamber. Two doses of MK16 BLNP-*ΔFosb* mRNA were intravenously administrated to the mice after each conditioning day. On day 4, during the post-test phase, the mice were given free access to both compartments and their time spent in each compartment was recorded as a measure of preference for the drug-paired side. As expected, the subthreshold dose of cocaine did not induce CPP in control PBS-treated animals (Fig. 5c). Importantly, mice receiving MK16 BLNP-*ΔFosb* mRNA exhibited a significant preference for the cocaine-associated compartment compared with the pre-test (Fig. 5c). This increase in preference indicates augmented drug-seeking behaviour in the MK16 BLNP-*ΔFosb*-treated mice, which is consistent with previous work that overexpressed ΔFOSB selectively in NAc neurons either in inducible transgenic mice or by viral-mediated gene transfer[49,52].

To further explore the clinical translatability of MK16 BLNP-*ΔFosb* mRNA, we examined MK16 BLNPs for the delivery of *ΔFosb* mRNA to adult human brain tissue ex vivo. Cortical tissue samples from two adult human subjects were treated with MK16 BLNP-*ΔFosb* mRNA (Fig. 5d). Quantitative analysis revealed ΔFOSB expression in 4.00 ± 0.99% of neurons, 6.49 ± 2.33% of astrocytes and 2.38 ± 0.94%

https://doi.org/10.1038/s41563-024-02114-5

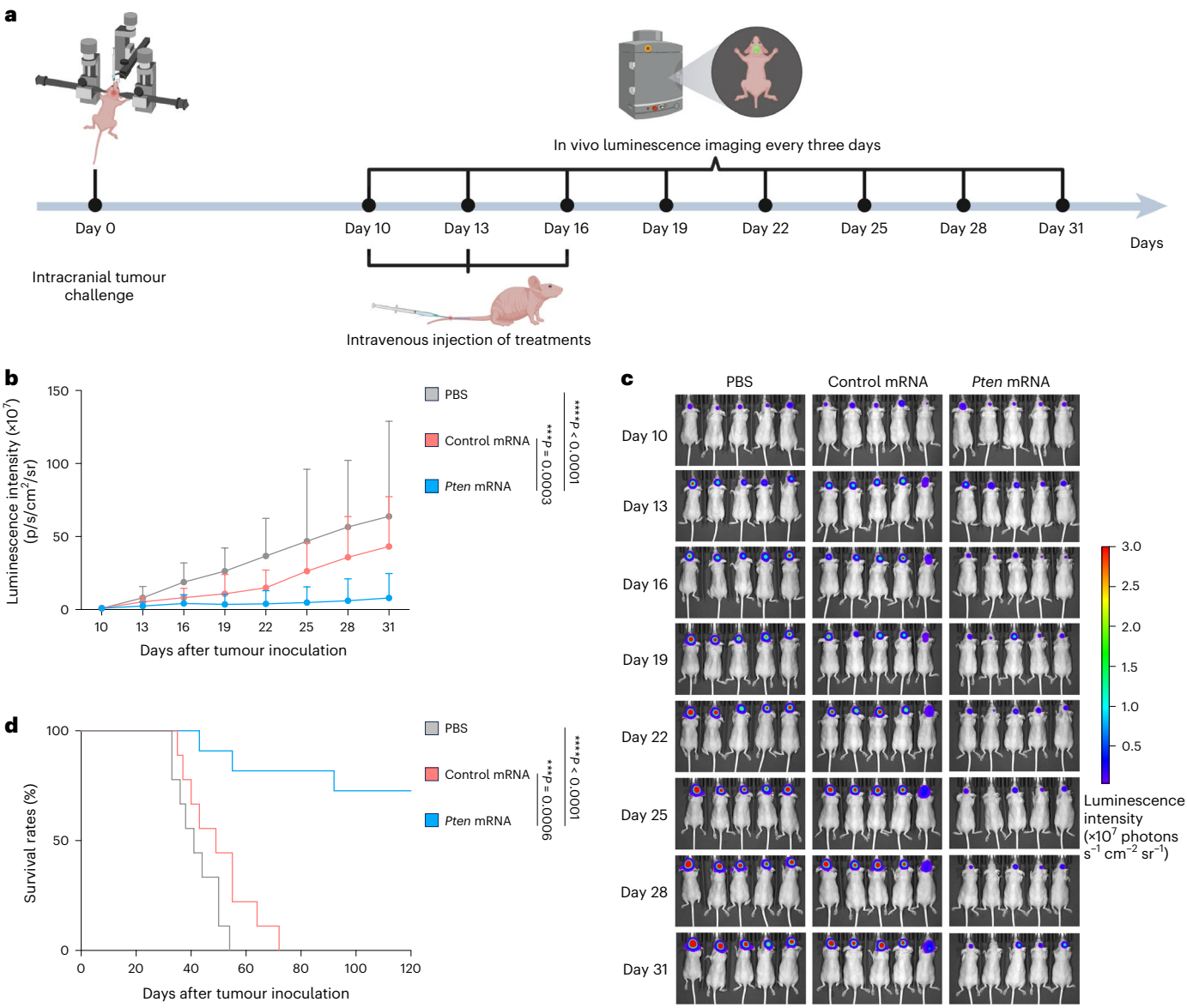

Fig. 6 | MK16 BLNP-*Pten* mRNA treatment in an orthotopic GBM mouse model. a, Schematic of the treatment regimen in the U-118MG GBM model. The treatments were intravenously injected into the tumour-bearing mice via the tail vein at an mRNA dose of 1.0 mg kg^{-1}. A total of three treatments were given at three-day intervals. **b**, Luminescence intensity of orthotopic GBM tumour tissues in the mice treated with PBS, MK16 BLNP-control mRNA and MK16 BLNP-*Pten* mRNA via the tail vein. **c**, Representative IVIS images of the tumour-bearing mice. **d**, Mouse survival over time. $n = 9$ mice for the PBS group and control mRNA group. $n = 10$ mice for the *Pten* mRNA group. Data in **b** are presented as the mean ± s.d. Statistical significance and *P* values in **b** were determined by two-way ANOVA with Fisher's least significant difference. Statistical significance and *P* values in **d** were analysed by the log-rank (Mantel–Cox) test. $^*P < 0.05$, $^{**}P < 0.01$, $^{***}P < 0.001$, $^{****}P < 0.0001$.

of microglia, whereas the untreated slices exhibited no detectable expression (Fig. 5e).

Efficacy of MK16 BLNPs for treating GBM

GBM represents the most aggressive and lethal form of primary brain tumour[53]. Owing to its rapid progression and poor prognosis, identifying effective therapeutic targets is crucial. A tumour suppressor gene, like phosphatase and tensin homologue (PTEN), is commonly mutated in wide ranges of GBM, which may be a great candidate for therapeutic intervention[27,54]. To investigate the clinical potential of MK16 BLNPs in treating PTEN-mutated GBM, we formulated MK16 BLNPs with *Pten* mRNA and intravenously administered this formulation to tumour-bearing immunodeficient mice in an orthotopic model of human U-118MG GBM (Fig. 6a). We first investigated the expression of PTEN after the treatment of MK16 BLNP-*Pten* mRNA in the orthotopic GBM tumour model. Immunofluorescence staining of brain sections containing GBM demonstrated greater accumulation of MK16 BLNP-*Pten* mRNA within the tumour region rather than adjacent normal tissue (Supplementary Fig. 18a). Moreover, MK16 BLNP-*Pten* mRNA reduced the tumour growth, thereby achieving prolonged survival in tumour-bearing mice compared with the PBS and MK16 BLNP-control mRNA (mCherry mRNA) groups (Fig. 6b–d). In particular, 70% of the mice treated with MK16 BLNP-*Pten* mRNA survived over 120 days in the orthotopic GBM model. Histological analysis revealed that mice treated with MK16 BLNP-*Pten* mRNA exhibited smaller residual tumours than both PBS group and MK16 BLNP-control mRNA group (Supplementary Fig. 18b). Additionally, mice treated with MK16 BLNP-*Pten* mRNA showed significantly reduced tumour growth and enhanced survival rates compared with those receiving MC3 LNP-*Pten* mRNA (Supplementary Fig. 19a–c).

These results demonstrate that the systemic delivery of MK16 BLNP-*Pten* mRNA is a promising strategy for effective GBM treatment. Together, the impressive effects of MK16 BLNPs in both cocaine addiction and GBM models establish its potential as a powerful delivery platform for studying and treating various brain disorders.

Outlook

Overall, we have designed and synthesized a library of BBB-crossing ionizable lipids by attaching a variety of lipid tails to different small molecules known for their ability to penetrate the BBB. MK16 BLNP, a lead material, is capable of crossing the BBB simultaneously mediated by caveolae and γ-secretase, enabling the efficient delivery of functional mRNA to several types of brain cell, and exhibiting tolerability under various dosing regimens. For future investigational new drug applications, it is crucial to conduct a toxicology study following good laboratory practice based on FDA guidelines, which provides a comprehensive understanding of the safety profile of MK16 BLNPs. For example, dose escalation studies and repeat administrations are essential to uncover the maximum-tolerated dose and potential long-term adverse effects. Additionally, specific mRNA cargoes need to be carefully designed and thoroughly examined to ensure precise targeting and efficacy in the treatment of the diverse pathophysiological mechanisms underlying various brain disorders. In summary, this BLNP platform represents an important proof-of-concept study to advance LNP-mRNA delivery to the brain, which offers a possible avenue for treating a wide range of brain disorders.

Online content

Any methods, additional references, Nature Portfolio reporting summaries, source data, extended data, supplementary information, acknowledgements, peer review information; details of author contributions and competing interests; and statements of data and code availability are available at https://doi.org/10.1038/s41563-024-02114-5.

References

1. Weissman, D. & Karikó, K. mRNA: fulfilling the promise of gene therapy. *Mol. Ther.* **23**, 1416–1417 (2015).
2. Pardi, N., Hogan, M. J., Porter, F. W. & Weissman, D. mRNA vaccines—a new era in vaccinology. *Nat. Rev. Drug Discov.* **17**, 261–279 (2018).
3. Hajj, K. A. & Whitehead, K. A. Tools for translation: non-viral materials for therapeutic mRNA delivery. *Nat. Rev. Mater.* **2**, 17056 (2017).
4. Hou, X., Zaks, T., Langer, R. & Dong, Y. Lipid nanoparticles for mRNA delivery. *Nat. Rev. Mater.* **6**, 1078–1094 (2021).
5. Chaudhary, N., Weissman, D. & Whitehead, K. A. mRNA vaccines for infectious diseases: principles, delivery and clinical translation. *Nat. Rev. Drug Discov.* **20**, 817–838 (2021).
6. Zhong, R. et al. Hydrogels for RNA delivery. *Nat. Mater.* **22**, 818–831 (2023).
7. Chen, S. et al. Nanotechnology-based mRNA vaccines. *Nat. Rev. Methods Prim.* **3**, 63 (2023).
8. Baden, L. R. et al. Efficacy and safety of the mRNA-1273 SARS-CoV-2 vaccine. *N. Engl. J. Med.* **384**, 403–416 (2020).
9. Polack, F. P. et al. Safety and efficacy of the BNT162b2 mRNA COVID-19 vaccine. *N. Engl. J. Med.* **383**, 2603–2615 (2020).
10. Wang, C., Zhang, Y. & Dong, Y. Lipid nanoparticle–mRNA formulations for therapeutic applications. *Acc. Chem. Res.* **54**, 4283–4293 (2021).
11. Zhang, Y., Sun, C., Wang, C., Jankovic, K. E. & Dong, Y. Lipids and lipid derivatives for RNA delivery. *Chem. Rev.* **121**, 12181–12277 (2021).
12. Cheng, Q. et al. Selective organ targeting (SORT) nanoparticles for tissue-specific mRNA delivery and CRISPR–Cas gene editing. *Nat. Nanotechnol.* **15**, 313–320 (2020).
13. Riley, R. S. et al. Ionizable lipid nanoparticles for in utero mRNA delivery. *Sci. Adv.* **7**, eaba1028 (2021).
14. Patel, S., Ryals, R. C., Weller, K. K., Pennesi, M. E. & Sahay, G. Lipid nanoparticles for delivery of messenger RNA to the back of the eye. *J. Control. Release* **303**, 91–100 (2019).
15. Qiu, M. et al. Lung-selective mRNA delivery of synthetic lipid nanoparticles for the treatment of pulmonary lymphangioleiomyomatosis. *Proc. Natl Acad. Sci. USA* **119**, e2116271119 (2022).
16. Melamed, J. R. et al. Ionizable lipid nanoparticles deliver mRNA to pancreatic β cells via macrophage-mediated gene transfer. *Sci. Adv.* **9**, eade1444 (2023).
17. Du, S. et al. Cholesterol-amino-phosphate (CAP) derived lipid nanoparticles for delivery of self-amplifying RNA and restoration of spermatogenesis in infertile mice. *Adv. Sci.* **10**, 2300188 (2023).
18. Xiong, B. et al. Strategies for structural modification of small molecules to improve blood–brain barrier penetration: a recent perspective. *J. Med. Chem.* **64**, 13152–13173 (2021).
19. Brown, K. M. et al. Expanding RNAi therapeutics to extrahepatic tissues with lipophilic conjugates. *Nat. Biotechnol.* **40**, 1500–1508 (2022).
20. Banks, W. A. From blood–brain barrier to blood–brain interface: new opportunities for CNS drug delivery. *Nat. Rev. Drug Discov.* **15**, 275–292 (2016).
21. Daneman, R., Zhou, L., Kebede, A. A. & Barres, B. A. Pericytes are required for blood–brain barrier integrity during embryogenesis. *Nature* **468**, 562–566 (2010).
22. Hawkins, B. T. & Davis, T. P. The blood-brain barrier/neurovascular unit in health and disease. *Pharmacol. Rev.* **57**, 173 (2005).
23. Nance, E., Pun, S. H., Saigal, R. & Sellers, D. L. Drug delivery to the central nervous system. *Nat. Rev. Mater.* **7**, 314–331 (2022).
24. Arvanitis, C. D., Ferraro, G. B. & Jain, R. K. The blood–brain barrier and blood–tumour barrier in brain tumours and metastases. *Nat. Rev. Cancer* **20**, 26–41 (2020).
25. Terstappen, G. C., Meyer, A. H., Bell, R. D. & Zhang, W. Strategies for delivering therapeutics across the blood–brain barrier. *Nat. Rev. Drug Discov.* **20**, 362–383 (2021).
26. Wang, Y. et al. Overcoming the blood–brain barrier for gene therapy via systemic administration of GSH-responsive silica nanocapsules. *Adv. Mater.* **35**, 2208018 (2022).
27. Yang, Z. et al. Large-scale generation of functional mRNA-encapsulating exosomes via cellular nanoporation. *Nat. Biomed. Eng.* **4**, 69–83 (2020).
28. Tylawsky, D. E. et al. P-selectin-targeted nanocarriers induce active crossing of the blood–brain barrier via caveolin-1-dependent transcytosis. *Nat. Mater.* **22**, 391–399 (2023).
29. Abbott, A. Levodopa: the story so far. *Nature* **466**, S6–S7 (2010).
30. Kageyama, T. et al. The 4F2hc/LAT1 complex transports L-DOPA across the blood–brain barrier. *Brain Res.* **879**, 115–121 (2000).
31. Hutchinson, K. et al. Describing inhibitor specificity for the amino acid transporter LAT1 from metainference simulations. *Biophys. J.* **121**, 4476–4491 (2022).
32. Wolosker, H., Blackshaw, S. & Snyder Solomon, H. Serine racemase: a glial enzyme synthesizing D-serine to regulate glutamate-*N*-methyl-D-aspartate neurotransmission. *Proc. Natl Acad. Sci. USA* **96**, 13409–13414 (1999).
33. Bodner, O. et al. D-Serine signaling and NMDAR-mediated synaptic plasticity are regulated by system A-type of glutamine/D-serine dual transporters. *J. Neurosci.* **40**, 6489 (2020).
34. Hatanaka, T. et al. Transport of D-serine via the amino acid transporter $ATB^{0,+}$ expressed in the colon. *Biochem. Biophys. Res. Commun.* **291**, 291–295 (2002).
35. Ganapathy, M. E. & Ganapathy, V. Amino acid transporter $ATB^{0,+}$ as a delivery system for drugs and prodrugs. *Curr. Drug Targets: Immune, Endocr. Metab. Disord.* **5**, 357–364 (2005).

36. Darlix, A. et al. Chemotherapy and diffuse low-grade gliomas: a survey within the European Low-Grade Glioma Network. *Neurooncol. Pract.* **6**, 264–273 (2019).
37. de Gooijer, M. C. et al. Improved brain penetration and antitumor efficacy of temozolomide by inhibition of ABCB1 and ABCG2. *Neoplasia* **20**, 710–720 (2018).
38. Carbonaro, T. M. & Gatch, M. B. Neuropharmacology of *N*,*N*-dimethyltryptamine. *Brain Res. Bull.* **126**, 74–88 (2016).
39. Ma, F. et al. Neurotransmitter-derived lipidoids (NT-lipidoids) for enhanced brain delivery through intravenous injection. *Sci. Adv.* **6**, eabb4429 (2020).
40. Nagai, F., Nonaka, R. & Satoh Hisashi Kamimura, K. The effects of non-medically used psychoactive drugs on monoamine neurotransmission in rat brain. *Eur. J. Pharmacol.* **559**, 132–137 (2007).
41. Yang, J. et al. Turn-on chemiluminescence probes and dual-amplification of signal for detection of amyloid beta species in vivo. *Nat. Commun.* **11**, 4052 (2020).
42. Cook, J. J. et al. Acute γ-secretase inhibition of nonhuman primate CNS shifts amyloid precursor protein (APP) metabolism from amyloid-β production to alternative APP fragments without amyloid-β rebound. *J. Neurosci.* **30**, 6743–6750 (2010).
43. Fouladi, M. et al. Phase I trial of MK-0752 in children with refractory CNS malignancies: a pediatric brain tumor consortium study. *J. Clin. Oncol.* **29**, 3529–3534 (2011).
44. Li, B. et al. An orthogonal array optimization of lipid-like nanoparticles for mRNA delivery in vivo. *Nano Lett.* **15**, 8099–8107 (2015).
45. Zou, Y. et al. Blood-brain barrier–penetrating single CRISPR-Cas9 nanocapsules for effective and safe glioblastoma gene therapy. *Sci. Adv.* **8**, eabm8011 (2022).
46. Madisen, L. et al. A robust and high-throughput Cre reporting and characterization system for the whole mouse brain. *Nat. Neurosci.* **13**, 133–140 (2010).
47. Cook, N. et al. A phase I trial of the γ-secretase inhibitor MK-0752 in combination with gemcitabine in patients with pancreatic ductal adenocarcinoma. *Br. J. Cancer* **118**, 793–801 (2018).
48. Krop, I. et al. Phase I pharmacologic and pharmacodynamic study of the gamma secretase (Notch) inhibitor MK-0752 in adult patients with advanced solid tumors. *J. Clin. Oncol.* **30**, 2307–2313 (2012).
49. Kelz, M. B. et al. Expression of the transcription factor ΔFosB in the brain controls sensitivity to cocaine. *Nature* **401**, 272–276 (1999).
50. Nestler, E. J., Barrot, M. & Self, D. W. ΔFosB: a sustained molecular switch for addiction. *Proc. Natl Acad. Sci. USA* **98**, 11042–11046 (2001).
51. Zhang, Y. et al. Overexpression of deltaFosB in nucleus accumbens mimics the protective addiction phenotype, but not the protective depression phenotype of environmental enrichment. *Front. Behav. Neurosci.* **8**, 297 (2014).
52. Robison, A. J. et al. Behavioral and structural responses to chronic cocaine require a feedforward loop involving ΔFosB and calcium/calmodulin-dependent protein kinase II in the nucleus accumbens shell. *J. Neurosci.* **33**, 4295–4307 (2013).
53. Weller, M. et al. Glioma. *Nat. Rev. Dis. Prim.* **10**, 33 (2024).
54. Hopkins, B. D., Hodakoski, C., Barrows, D., Mense, S. M. & Parsons, R. E. PTEN function: the long and the short of it. *Trends Biochem. Sci.* **39**, 183–190 (2014).

[1]Icahn Genomics Institute, Precision Immunology Institute, Department of Immunology and Immunotherapy, Department of Oncological Sciences, Tisch Cancer Institute, Biomedical Engineering and Imaging Institute, Friedman Brain Institute, Icahn School of Medicine at Mount Sinai, New York, NY, USA. [2]Division of Pharmaceutics and Pharmacology, College of Pharmacy, The Ohio State University, Columbus, OH, USA. [3]Nash Family Department of Neuroscience and Friedman Brain Institute, Icahn School of Medicine at Mount Sinai, New York, NY, USA. [4]Center for Electron Microscopy and Analysis, The Ohio State University, Columbus, OH, USA. [5]Department of Materials Science and Engineering, The Ohio State University, Columbus, OH, USA. [6]Department of Oncological Sciences, The Tisch Cancer Institute, Icahn School of Medicine at Mount Sinai, New York, NY, USA. [7]Biogen, Cambridge, MA, USA. [8]Charles Bronfman Institute for Personalized Medicine, Department of Neurosurgery, Icahn School of Medicine at Mount Sinai, New York, NY, USA. [9]These authors contributed equally: Chang Wang, Yonger Xue, Tamara Markovic. ✉e-mail: eric.nestler@mssm.edu; paul.peng@biogen.com; yizhou.dong@mssm.edu

Methods

Animal studies

The animal experiments conducted in this study adhered to the guidelines approved by the Institutional Animal Care and Use Committee of the Ohio State University (2014A00000106) and the Icahn School of Medicine at Mount Sinai (IPROTO202200000134). All relevant ethical regulations were followed as applicable. Both male and female C57BL/6J (000664), Ai14 (007914) and NU/J mice (002019) (6–10 weeks old), obtained from the Jackson Laboratory, were used for the experiments.

Materials

All chemicals were purchased from Fisher Scientific unless otherwise listed. DOPE (850725), 1,2-distearoyl-*sn*-glycero-3-phosphocholine (DSPC, 850365) and DMG-PEG_{2k} (880151) were purchased from Avanti Polar Lipids. MC3 (555308), ALC-0315 (556006), ALC-0159 (556014) and SM-102 (464358) were purchased from MedKoo Biosciences. NGST (HY-15185) and MK-0752 (HY-10974) were obtained from MedChemExpress. 5-(*N*-Ethyl-*N*-isopropyl)-amiloride (A3085), MβCD (C4555) and chlorpromazine (1125006) were purchased from Sigma-Aldrich. The detailed synthesis of all the BLs is described in the Supplementary Information. The ^{1}H nuclear magnetic resonance spectra and mass spectra of all BLs are shown in Supplementary Figs. 20–52. The mRNAs encoded with FLuc, GFP, Cre recombinase, *ΔFosb-FLAG* and *Pten-FLAG* used in this study were constructed according to previously reported procedures[55]. Minimum essential medium (11095080), Dulbecco's modified Eagle's medium (11965092), neurobasal medium (21103049), N-2 supplement (17502048), B-27 supplement (17504044) and heat-inactivated foetal bovine serum (A5670801) were obtained from Thermo Fisher Scientific. Human-brain-derived neurotrophic factor (78005) was purchased from STEMCELL Technologies. The N2a (CCL-131) and bEnd.3 (CRL-2299) cells were obtained from the American Type Culture Collection.

Preparation and characterization of BLNPs

A previously reported method was used to prepare BLNPs encapsulating mRNA[55]. BLs were formulated with DOPE, Chol and DMG-PEG_{2k} using BL/DOPE/cholesterol/DMG-PEG_{2k} at a molar ratio of 20/30/40/0.75. The original mass ratio of ionizable lipid/mRNA in the formulation is 10. The MC3 lipid was formulated with DSPC, Chol and DMG-PEG_{2k} at a molar ratio of MC3/DSPC/Chol/DMG-PEG_{2k} = 50/10/38.5/1.5. For ALC-0315 and SM-102, the formulation ratio is ALC-0315/DSPC/Chol/ALC-0159 = 46.3/9.4/42.7/1.6 and SM-102/DSPC/Chol/DMG-PEG_{2k} = 50:10:38.5:1.5, respectively. The hydrodynamic diameter and polydispersity of the formulated BLNPs were measured by a Nano ZS Zetasizer (Malvern). The encapsulation efficiency was measured using the RiboGreen assay. The morphology of BLNPs was visualized using cryogenic transmission electron microscopy (Thermo Scientific Glacios) as previously described[44].

In vitro luciferase assay for BLNPs

The N2a cells were cultured in minimum essential medium with 10% foetal bovine serum (37 °C, 5% CO_2) and the bEnd.3 cells were cultured in Dulbecco's modified Eagle's medium with 10% foetal bovine serum (37 °C, 5% CO_2). The cells were seeded in white 96-well plates (2×10^4 cells per well), followed by overnight incubation in the growth medium. Then, 5 µl of BLNPs loaded with FLuc mRNA (0.01 mg ml^{-1} FLuc mRNA) were added to each well. Following an 18 h incubation period, cells were treated with a Bright-Glo luciferase substrate. After 5 min incubation, the relative luminescence intensity was quantified using a BioTek Cytation 5 Cell Imaging Multimode Reader.

Cytotoxicity of BLNPs in vitro

To assess the cytotoxicity of all BLNPs in N2a cells and bEnd.3 cells, a modified version of the MTT assay was used. After seeding in a 96-well plate and culturing overnight, the N2a cells and bEnd.3 cells were treated with either PBS or the selected BLNPs for 24 h. Afterwards, the MTT reagents were added to the cells and then further incubated at 37 °C for 4 h. Subsequently, dimethyl sulfoxide was substituted for the old growth medium, followed by a 10 min shaking period. A wavelength of 570 nm was used to quantify absorbance.

BLNP-FLuc mRNA delivery by intravenous administration via tail vein

C57BL/6J mice (n = 3 for each group) were intravenously injected with selected BLNPs (N^1-methyl-pseudouridine FLuc mRNA, 0.5 mg kg^{-1}). After 6 h, the mice received an intraperitoneal injection of 150 µl of D-luciferin substrate (30 mg ml^{-1}). The major organs, including the brain, were dissected and imaged after 8 min using a Xenogen IVIS imaging system. The signals in the brain of all the groups were quantified using regions of interest and then the signals of the treatment groups were divided by the average signal intensity of the control groups for normalization. To investigate the in vivo kinetics of MK16 BLNPs, C57BL/6J mice (n = 3 for each group) were intravenously injected with MK16 BLNPs encapsulating Alexa Fluor 647-labelled RNA at the RNA dose of 0.5 mg kg^{-1}. After 1, 6, 18, 24 and 48 h, the brains were dissected from mice and immediately imaged using a Xenogen IVIS imaging system. To examine the in vivo biodistribution of MK16 BLNPs, C57BL/6J mice (n = 3 for each group) were intravenously administered with MK16 BLNP-Alexa Fluor 647-labelled RNA at an RNA dose of 0.5 mg kg^{-1}. After 1 h, major organs including brains were dissected from mice and immediately imaged using a Xenogen IVIS imaging system.

Immunofluorescence staining for brain tissues

After 24 h post-treatment (*ΔFosb* mRNA delivery study) or 5 days after the last dose (Cre mRNA delivery study), mice were transcardially perfused with 20 ml of PBS and then 20 ml of 4% paraformaldehyde. The mouse brains were post-fixed in 4% paraformaldehyde at 4 °C overnight and then incubated in a 25% sucrose solution in PBS at 4 °C for up to 3 days before the section. Coronal sections of the brains were taken (5–10 µm thick) using cryotome, mounted on microscope slides and then incubated in 10% goat serum and 0.3% Triton X-100 in PBS for 1 h. For *ΔFosb* mRNA delivery study, the brain slices were stained with anti-DDDDK tag (1:200, Abcam, ab205606) overnight at 4 °C, whereas for the Cre mRNA delivery study, the slices were stained with the primary antibodies including anti-GFAP (1:200, Abcam, ab68428) and anti-MAP2 (1:200, Abcam, ab183830). After rinsing with PBS, secondary antibodies (donkey anti-rabbit IgG H&L (Alexa Fluor 488) (1:200, Abcam, ab150073) and donkey anti-rabbit IgG H&L (Alexa Fluor 647) (1:200, Abcam, ab150075)) were used for 60 min incubation at room temperature. 4′,6-Diamino-2-phenylindole dihydrochloride (DAPI, Thermo) was used as a nuclear counterstain. All sections were imaged using fluorescence microscopy (Leica DiM8). To quantify the expression of tdTomato in specific cell types, all cells were first identified using DAPI staining. Subsequently, cells expressing tdTomato, MAP2 (a marker for neurons) and GFAP (a marker for astrocytes) were counted within the total cell population. The proportion of tdTomato positivity was then determined by dividing the number of tdTomato-positive cells by the number of cells positive for either Map2 or GFAP. This approach allows for the calculation of tdTomato expression levels specifically in neurons and astrocytes.

Immunofluorescence flow cytometry for brain cells

The dissociation and collection of brain cells followed established protocols with minor modifications[56]. After 12 h post-treatment (GFP mRNA delivery study) or 5 days after the last dose (Cre mRNA delivery study), mice were anaesthetized and transcardially perfused with 20 ml PBS, and then the brain was carefully dissected. After removing the meninges, the brain tissue was dissected into small pieces in the TrypLE Express Enzyme (1×) solution containing 10 U ml^{-1} DNase I and then incubated at 37 °C for 15 min. Brain tissues were mechanically dissociated by pipetting to obtain a uniform suspension. Then, single

cells were obtained using a cell strainer 70 µm nylon mesh (Fisher) and purified with myelin removal beads based on the manufacturer's protocols (Myelin Removal Beads II, human, mouse, rat, 130-096-433; Miltenyi Biotec). The purified single-cell solutions were then prepared for immunofluorescence staining separately with specific cell markers (primary antibodies) for 1 h at 4 °C: NeuN (1:100, Abcam, ab177487) for neurons, GFAP (1:100, Abcam, ab68428) for astrocytes, CD11b (1:100, Abcam, ab184308) for microglia, CD31 (1:100, Abcam, ab134168) for BCECs, platelet-derived growth factor receptor alpha (1:100, Abcam, ab203491) for oligodendrocytes and Islet-1 (1:100, Abcam, ab109517) for neural stem cells. For staining with NeuN, GFAP or Islet-1, the cells were fixed and permeabilized using eBioscience intracellular fixation and permeabilization buffer set for intracellular staining. The cells were then stained with secondary antibodies (donkey anti-rabbit IgG H&L (Alexa Fluor 647) (1:200, Abcam, ab150075)) for 30 min at 4 °C. All samples were then fixed and permeabilized for GFP staining (Alexa Fluor 488) (1:200, BioLegend, FM264G). After the final wash of antibody staining, the cells were stained by a DAPI staining solution (Miltenyi Biotec) and proceeded directly to flow cytometry analysis, where 20,000 DAPI+ events were recorded.

CPP

An unbiased CPP test was carried out as described[52] using three chambered CPP boxes (Med Associates) and software in which two larger end chambers have distinct visual (grey versus striped walls) and tactile (small grid versus large grid flooring) cues to allow differentiation. All experimental sessions were conducted in a room with dim lighting and controlled ambient temperature. During the initial pre-test session, mice were permitted to freely explore all the three chambers for 20 min to ensure no inherent preference for any chamber. To mitigate any pre-existing bias towards a particular chamber, the groups were carefully balanced. The conditioning phase involved associating one end chamber with a saline injection in the morning and the opposite end chamber with a cocaine injection (12.5 mg kg^{-1}) in the afternoon, over two consecutive days. Each conditioning session lasted for 30 min. Two doses of MK16 BLNP-*ΔFosb* mRNA (1 mg kg^{-1}) were intravenously injected into the mice on conditioning days 2 and 3. On the fourth day, the CPP test was administered, allowing each mouse to move freely among all three chambers for 20 min. The place preference scores were calculated based on the difference in time spent on the side paired with cocaine versus the side paired with saline.

Ex vivo mRNA delivery in human brain tissue

All research involving human subjects was conducted under STUDY-13-00415 of the Human Research Protection Program at the Icahn School of Medicine at Mount Sinai. Human cortical tissues were obtained with consent from two adult patients with Parkinson's disease during routine neurosurgery for the implantation of deep brain stimulation electrodes. During deep brain stimulation surgery, a standard, FDA-approved technique known as cauterization is used to assist in the safe implantation of the deep brain stimulation electrode. The cauterization technique results in a small volume loss of 'non-eloquent' cortical tissue, which means that the loss has no discernable functional impact on the patient. As part of the living brain project (STUDY-13-00415) protocol, this technique was adapted to retrieve a small biopsy from the prefrontal cortex region, which would otherwise have been discarded post-cauterization. The biopsy of the prefrontal cortex is taken using a 4 mm biopsy punch and a microdissector before cauterization. The obtained cortical tissue biopsies were promptly stored on ice and sectioned into 300-µm-thick slices within 30 min. The slices were then cultured in a neurobasal medium containing 1% N-2, 1% B-27 and 10 ng ml^{-1} human-brain-derived neurotrophic factor for 1 h before treatment with 1 µg MK16 BLNP-*ΔFosb* mRNA. After 24 h, the slices were dissociated into a single-cell suspension and prepared for immunofluorescence staining with specific cell markers.

In vivo mRNA delivery for GBM treatment

The U-188 MG cell line (HTB-15, ATCC) was transduced with FLuc-IRES-Puro Lentivirus (GlowCell-14p, Biosettia) based on the manufacturer's guidance to generate the U-118MG-FLuc cell line. To establish an orthotopic GBM model, each mouse received an injection of pain killer (buprenorphine 0.1 mg kg^{-1}) 30 min before deep anaesthesia (induction at 4% isoflurane; maintenance at 1.5% isoflurane). The mice were positioned into a stereotaxic frame (David Kopf Instruments) and their body temperatures were maintained using a heating pad. Skin was disinfected three times with 70% ethanol before skin incision. Single burr holes (diameter, 1.0 mm) were drilled at the following coordinates: $X = -1.0$ mm, $Y = +1.5$ mm. U-118MG-FLuc cells (1×10^6) were slowly injected at a constant rate of 300 nl min^{-1} (2 µl per site) into the lateral of the hippocampus ($X = -1.0$ mm, $Y = +1.5$ mm, $Z = +1.6$ mm) using a motorized micro-pump (Legato 130, KD Scientific) with a precision syringe (Hamilton Gastight Series, 10 µl). Before pulling out the syringe, it was maintained for 3 min. Then, the mice skin was disinfected again, and the skin was closed by surgical staples. All mice were closely monitored until they were awake in a 37 °C heating chamber.

The establishment of orthotopic U-118MG-FLuc brain tumour using a Xenogen IVIS imaging system after 10 days post-implantation. To examine the accumulation of MK16 BLNP-*Pten* mRNA in the GBM region, mice with established U-118MG GBM were administered MK16 BLNP-*Pten* mRNA intravenously (via the tail vein; 1.0 mg kg^{-1}). After 24 h, the mice were transcardially perfused with 20 ml PBS. The brains were then carefully dissected, fixed and sectioned. Brain slices were stained overnight at 4 °C with an anti-DDDDK tag antibody (1:200, Abcam, ab205606), followed by a 60 min incubation with a secondary antibody (donkey anti-rabbit IgG H&L (Alexa Fluor 488), 1:200, Abcam, ab150073) at room temperature. DAPI was used to counterstain the nuclei, and all the sections were imaged using fluorescence microscopy (Leica DiM8). The mice were divided into three random groups: PBS group, control (mCherry) mRNA group and *Pten* mRNA group. Treatments were intravenously administered via the tail vein on days 10, 13 and 16, with doses of PBS, MK16 BLNP-control mRNA (or MC3 LNP-*Pten* mRNA) and MK16 BLNP-*Pten* mRNA at 1.0 mg kg^{-1}, respectively. From days 10 to 31, the mice were imaged every 3 days to measure the luciferase intensity of the brain tumours. The mice were then continuously monitored, and those exhibiting loss of body weight of 20% or body condition score of ≤2 were humanely removed from the study. To visualize the tumour residues, the brain tissues were dissected, fixed and sectioned. The brain slices were counterstained with DAPI to distinguish between the tumour and normal tissue regions.

Statistics and reproducibility

The statistical analysis was conducted using GraphPad Prism 9 software, Microsoft Excel (v. 2112), ImageJ (v. 1.53) and FlowJo (v. 10.4). For comparison between multiple data groups, one-way analysis of variance (ANOVA) followed by Dunnett's multiple comparisons test were used. The two-tailed Student's *t*-test was used to compare two data groups. For the CPP model, two-way ANOVA with Šidák post hoc test were used. In the GBM model, two-way ANOVA with Fisher's least significant difference was used to compare the luminescence intensity and the log-rank (Mantel–Cox) test was conducted to compare the survival rates. *P* values of <0.05 were considered statistically significant. All the data met the assumptions of the statistical tests used, including normality and equal variances, and were formally tested to ensure the validity of the statistical analysis. No statistical method was used to predetermine the sample size.

Ethics statement

All research involving human subjects was carried out under STUDY-13-00415 of the Human Research Protection Program at the Icahn School of Medicine at Mount Sinai. Research participants in the living cohort provided informed consent for sample collection, genomic profiling,

clinical data extraction from medical records and public sharing of deidentified data.

Reporting summary

Further information on research design is available in the Nature Portfolio Reporting Summary linked to this article.

Data availability

Mouse reference genome assembly GRCm38.99 was used for data analysis (https://hgdownload.soe.ucsc.edu/goldenPath/mm10/chromosomes/). All data supporting the findings of this study are available within the Article and its Supplementary Information. Source data are provided with this paper.

References

55. Xue, Y. et al. LNP-RNA-engineered adipose stem cells for accelerated diabetic wound healing. *Nat. Commun.* **15**, 739 (2024).
56. Ouellette, J. & Lacoste, B. Isolation and functional characterization of primary endothelial cells from mouse cerebral cortex. *STAR Protoc.* **2**, 101019 (2021).

Acknowledgements

Y.D. acknowledges support from the Maximizing Investigators' Research Awards (R35GM144117) from the National Institute of General Medical Sciences, the fund from the Icahn School of Medicine at Mount Sinai and generous support from Biogen. E.J.N. acknowledges support from the National Institute on Drug Abuse (P01DA047233). Cryo-electron microscopy was performed at the Center for Electron Microscopy and Analysis (CEMAS) at The Ohio State University. We acknowledge E. Purisic and J. Dai for sharing the vibratome and providing instructions. We acknowledge the use of BioRender.com to prepare certain figures.

Author contributions

C.W., Y.X. and T.M. conceived the work, performed the experiments, analysed the data and wrote the paper. H.L., S.W., Y. Zhong, S.D., X.H., Z.L., M.T., Y. Zhang, L.W., K.G., A.M.M.-T. and L.M.H. contributed to the animal studies. Y.Y. contributed to the RNA-sequencing analysis. D.D.K., D.C. and J.Y. contributed to the mRNA synthesis. B.D. and D.W.M. contributed to the cryo-EM imaging. R.E.P. and J.P. contributed to the data analysis and manuscript editing. A.H., B.H.K. and A.W.C. contributed to the collection of human brain tissues. E.J.N., P.C.P. and Y.D. conceived and supervised the project and wrote the paper. The final paper was edited and approved by all authors.

Competing interests

Y.D. is a scientific advisor in Arbor Biotechnologies, Sirnagen Therapeutics and Moonwalk Biosciences, and also a co-founder and holds equity in Immunanoengineering Therapeutics. J.P. is a current employee of Biogen with salary and stock options. P.C.P. is a current employee of City Therapeutics with salary and stock options. The other authors declare no competing interests.

Additional information

Supplementary information The online version contains supplementary material available at https://doi.org/10.1038/s41563-024-02114-5.

Correspondence and requests for materials should be addressed to Eric J. Nestler, Paul C. Peng or Yizhou Dong.

Peer review information *Nature Materials* thanks Eden Tanner and the other, anonymous, reviewer(s) for their contribution to the peer review of this work.

nature portfolio

Corresponding author(s): Dr. Eric J. Nestler, Dr. Paul C. Peng & Dr. Yizhou Dong

Last updated by author(s): Nov 11, 2024

Reporting Summary

Nature Portfolio wishes to improve the reproducibility of the work that we publish. This form provides structure for consistency and transparency in reporting. For further information on Nature Portfolio policies, see our Editorial Policies and the Editorial Policy Checklist.

Statistics

For all statistical analyses, confirm that the following items are present in the figure legend, table legend, main text, or Methods section.

n/a	Confirmed	
☐	☒	The exact sample size (*n*) for each experimental group/condition, given as a discrete number and unit of measurement
☐	☒	A statement on whether measurements were taken from distinct samples or whether the same sample was measured repeatedly
☐	☒	The statistical test(s) used AND whether they are one- or two-sided *Only common tests should be described solely by name; describe more complex techniques in the Methods section.*
☐	☒	A description of all covariates tested
☐	☒	A description of any assumptions or corrections, such as tests of normality and adjustment for multiple comparisons
☐	☒	A full description of the statistical parameters including central tendency (e.g. means) or other basic estimates (e.g. regression coefficient) AND variation (e.g. standard deviation) or associated estimates of uncertainty (e.g. confidence intervals)
☐	☒	For null hypothesis testing, the test statistic (e.g. *F*, *t*, *r*) with confidence intervals, effect sizes, degrees of freedom and *P* value noted *Give P values as exact values whenever suitable.*
☒	☐	For Bayesian analysis, information on the choice of priors and Markov chain Monte Carlo settings
☒	☐	For hierarchical and complex designs, identification of the appropriate level for tests and full reporting of outcomes
☒	☐	Estimates of effect sizes (e.g. Cohen's *d*, Pearson's *r*), indicating how they were calculated

Our web collection on statistics for biologists contains articles on many of the points above.

Software and code

Policy information about availability of computer code

Data collection	6210 TOF LC/MS (Agilent), microFlex LRF MALDI-TOF-MS (Bruker Daltonics), Avance 400 MHz NMR (Bruker), Living Image® (4.8.2), Thermo Scientific EPU software (3.6), Nikon A1R Live Cell Imaging Confocal Microscope, LSRFortessa Flow Cytometer (BD Biosciences), BioTek CYTATION 5 plate reader, Fluorescence microscope (Leica DiM8), Malvern Zetasizer NanoZS, ChemDraw (RRID:SCR_016768), and Microsoft Excel (Version 2112)
Data analysis	GraphPad Prism 9, Microsoft Excel (Version 2112), ImageJ (Version 1.53) and FlowJo (Version 10.4).

For manuscripts utilizing custom algorithms or software that are central to the research but not yet described in published literature, software must be made available to editors and reviewers. We strongly encourage code deposition in a community repository (e.g. GitHub). See the Nature Portfolio guidelines for submitting code & software for further information.

Data

Policy information about availability of data

All manuscripts must include a data availability statement. This statement should provide the following information, where applicable:

- Accession codes, unique identifiers, or web links for publicly available datasets
- A description of any restrictions on data availability
- For clinical datasets or third party data, please ensure that the statement adheres to our policy

Mouse reference genome assembly GRCm38.99 was used for data analysis (https://hgdownload.soe.ucsc.edu/goldenPath/mm10/chromosomes/). The authors declare that all data supporting the findings of this study are available within the paper and Supplementary Information files. Source data are provided with this paper.

Field-specific reporting

Please select the one below that is the best fit for your research. If you are not sure, read the appropriate sections before making your selection.

☒ Life sciences ☐ Behavioural & social sciences ☐ Ecological, evolutionary & environmental sciences

For a reference copy of the document with all sections, see nature.com/documents/nr-reporting-summary-flat.pdf

Life sciences study design

All studies must disclose on these points even when the disclosure is negative.

Sample size	Standard number of replication is 3 in all in vitro studies. A minimum of 3 biological repeats is applied to evaluate significance. A minimum of 3 mice were used for in vivo studies. No sample size calculation was performed, but this sample size has been shown to be sufficient to ensure reproducibility in our previous studies.
Data exclusions	No animals or data were excluded from the analyses.
Replication	All experiments were performed at least in triplicates, and all attempts at replication were successful.
Randomization	Samples were randomly allocated to corresponding experimental groups.
Blinding	Researchers were not blinded for chemical synthesis because they need to take care of different experimental conditions. Experiments including flow assays, immunofluorescence imaging and animal experiments were performed by multiple researchers, who had minimal information of sample identification.

Reporting for specific materials, systems and methods

We require information from authors about some types of materials, experimental systems and methods used in many studies. Here, indicate whether each material, system or method listed is relevant to your study. If you are not sure if a list item applies to your research, read the appropriate section before selecting a response.

Materials & experimental systems

n/a	Involved in the study
☐	☒ Antibodies
☐	☒ Eukaryotic cell lines
☒	☐ Palaeontology and archaeology
☐	☒ Animals and other organisms
☐	☒ Human research participants
☒	☐ Clinical data
☒	☐ Dual use research of concern

Methods

n/a	Involved in the study
☒	☐ ChIP-seq
☐	☒ Flow cytometry
☒	☐ MRI-based neuroimaging

Antibodies

Antibodies used	Primary antibodies used for immunofluorescence staining: Rabbit recombinant Anti-MAP2 antibody [EPR19691] (Abcam, ab183830), 1: 200 dilution Rabbit recombinant Anti-GFAP antibody [EPR1034Y] (Abcam, ab68428), 1: 200 dilution Rabbit Recombinant Anti-DDDDK tag antibody [EPR20018-251] (Abcam, ab205606), 1:200 dilution Primary antibodies used for flow cytometry: Rabbit Recombinant Anti-NeuN antibody [EPR12763] (Abcam, ab177487), 1: 100 dilution Rabbit recombinant Anti-GFAP antibody [EPR1034Y] (Abcam, ab68428), 1: 100 dilution Rabbit Recombinant Anti-CD11b antibody [EPR19387] (ab184308), 1: 100 dilution Rabbit Recombinant Anti-CD31 antibody [EP3095] (Abcam, ab134168), 1: 100 dilution Rabbit Recombinant Anti-PDGFR alpha antibody [EPR22059-270] (Abcam, ab203491), 1: 100 dilution Rabbit Recombinant Anti-Islet 1 antibody [EP4182] (Abcam, ab109517),1: 100 dilution Rabbit Recombinant Anti-DDDDK tag antibody [EPR20018-251] (Abcam, ab205606), 1:100 dilution Alexa Fluor® 488 anti-GFP Antibody (Biolegend, FM264G), 1:200 dilution. Second antibodies: Donkey Anti-Rabbit IgG H&L (Alexa Fluor® 647) (Abcam, ab150075), 1:200 dilution Donkey Anti-Rabbit IgG H&L (Alexa Fluor® 488) (Abcam, ab150073), 1:200 dilution
Validation	These antibodies have been verified by the supplier and reported for the use in flow cytometry and IF. All the antibodies used are from commercial sources and validation data are available on the manufacturer's website based on their catalogue numbers. The

manufacturers include Abcam and Biolegend.
Rabbit recombinant Anti-MAP2 antibody [EPR19691] (Abcam, ab183830): https://www.abcam.com/en-us/products/primary-antibodies/map2-antibody-epr19691-ab183830
Rabbit Recombinant Anti-DDDDK tag antibody [EPR20018-251] (Abcam, ab205606): https://www.abcam.com/en-us/products/primary-antibodies/ddddk-tag-binds-to-flag-tag-sequence-antibody-epr20018-251-ab205606
Rabbit Recombinant Anti-NeuN antibody [EPR12763] (Abcam, ab177487): https://www.abcam.com/en-us/products/primary-antibodies/neun-antibody-epr12763-neuronal-marker-ab177487
Rabbit recombinant Anti-GFAP antibody [EPR1034Y] (Abcam, ab68428): https://www.abcam.com/en-us/products/primary-antibodies/gfap-antibody-epr1034y-ab68428
Rabbit Recombinant Anti-CD11b antibody [EPR19387] (Abcam, ab184308): https://www.abcam.com/en-us/products/primary-antibodies/cd11b-antibody-epr19387-ab184308
Rabbit Recombinant Anti-CD31 antibody [EP3095] (Abcam, ab134168): https://www.abcam.com/en-us/products/primary-antibodies/cd31-antibody-ep3095-ab134168
Rabbit Recombinant Anti-PDGFR alpha antibody [EPR22059-270] (Abcam, ab203491): https://www.abcam.com/en-us/products/primary-antibodies/pdgfr-alpha-antibody-epr22059-270-ab203491
Rabbit Recombinant Anti-Islet 1 antibody [EP4182] (Abcam, ab109517): https://www.abcam.com/en-us/products/primary-antibodies/islet-1-antibody-ep4182-neural-stem-cell-marker-ab109517
Alexa Fluor® 488 anti-GFP Antibody (Biolegend, FM264G): https://www.biolegend.com/ja-jp/products/alexa-fluor-488-anti-gfp-antibody-9584
Donkey Anti-Rabbit IgG H&L (Alexa Fluor® 647) (Abcam, ab150075): https://www.abcam.com/en-us/products/secondary-antibodies/donkey-rabbit-igg-h-l-alexa-fluor-647-ab150075
Donkey Anti-Rabbit IgG H&L (Alexa Fluor® 488) (Abcam, ab150073): https://www.abcam.com/en-us/products/secondary-antibodies/donkey-rabbit-igg-h-l-alexa-fluor-488-ab150073

Eukaryotic cell lines

Policy information about cell lines

Cell line source(s)	Neuro-2a cells, bEnd.3 cells and U-118MG cells were purchased from American Type Culture Collection (ATCC).
Authentication	Cell lines were not independently authenticated.
Mycoplasma contamination	Cell lines do not have mycoplasma contamination.
Commonly misidentified lines (See ICLAC register)	No commonly misidentified cell lines were used.

Animals and other organisms

Policy information about studies involving animals; ARRIVE guidelines recommended for reporting animal research

Laboratory animals	Both male and female C57BL/6 (000664), Ai14 (007914) and NU/J (002019) (6–10 weeks) were purchased from the Jackson Laboratory. All mice were housed in The Ohio State University (2014A00000106) or in The Icahn School of Medicine at Mount Sinai (IPROTO202200000134). All mouse studies were approved by the Institutional Animal Care and Use Committee (IACUC) and complied with local, state, and federal regulations. Mice were housed under a barrier environment (~20°C, ~45% humidity, and 12/12 light/dark cycle).
Wild animals	The study did not involve wild animals.
Field-collected samples	The study did not involve samples collected from field.
Ethics oversight	All mouse studies were approved by the Institutional Animal Care and Use Committee at The Ohio State University (2014A00000106) and The Icahn School of Medicine at Mount Sinai (IPROTO202200000134).

Note that full information on the approval of the study protocol must also be provided in the manuscript.

Human research participants

Policy information about studies involving human research participants

Population characteristics	All participants are patients of Dr. Brian Kopell, MD., who are committed to undergo the deep brain stimulation (DBS) implantation procedure to treat a neuropsychiatric disorder such as Parkinson's Disease, Dystonia, or Essential Tremor at Mount Sinai West (MSW). Participants must be 18 years or older and speak English or Spanish as their primary language.
Recruitment	All patients of Dr. Brian Kopell, MD., who are committed to undergo the DBS procedure at MSW to treat a neuropsychiatric disorder are eligible to participate in The Living Brain Project (LBP, STUDY-13-00415) study. Patients are presented with information about the study and are given the opportunity to participate during their pre-op meetings. To enroll, all patients must participate in the LBP Clinical Module, which allows for their Electronic Medical Record to be reviewed by the study team. Patients are also given the option to participate in two additional modules: LBP Biobank Module, which encompasses a sample collection (brain tissue and blood), and the LBP Neurophysiology Module, during which brain activity is recorded, mid-procedure, while the patient plays a game. Patients may end their participation at any time.
Ethics oversight	All human subjects research was carried out under STUDY-13-00415 of the Human Research Protection Program at the Icahn

Ethics oversight	School of Medicine at Mount Sinai. Research participants in the living cohort provided informed consent for sample collection, genomic profiling, clinical data extraction from medical records, and public sharing of de-identified data.

Note that full information on the approval of the study protocol must also be provided in the manuscript.

Flow Cytometry

Plots

Confirm that:

☒ The axis labels state the marker and fluorochrome used (e.g. CD4-FITC).

☒ The axis scales are clearly visible. Include numbers along axes only for bottom left plot of group (a 'group' is an analysis of identical markers).

☒ All plots are contour plots with outliers or pseudocolor plots.

☒ A numerical value for number of cells or percentage (with statistics) is provided.

Methodology

Sample preparation	Brain tissues were enzymatically dissociated to generate cell suspension. For intracellular staining, the cells were treated by fixation and permeation buffers before antibody staining.
Instrument	LSRFortessa Flow Cytometer (BD Biosciences)
Software	FlowJo (Version 10.4)
Cell population abundance	The cell abundance was shown in the results.
Gating strategy	For all flow cytometry experiments, the forward and side scatter properties were used to determine the 'Cell' gating and confirmed by positive labeling with nuclear DAPI staining. The cell markers used for subsequent gating were: NeuN for neurons, GFAP for astrocytes, CD11b for microglia, CD31 for brain capillary endothelial cell (BCEC), Platelet-derived growth factor receptor alpha (PDGFRα) for oligodendrocyte Islet-1 for neural stem cell (NSC). Positive populations were determined by comparing experimental samples against unstained controls.

☒ Tick this box to confirm that a figure exemplifying the gating strategy is provided in the Supplementary Information.